

**MAGNETIC RESONANCE IMAGE SEGMENTATION USING PULSE  
COUPLED NEURAL NETWORKS**

by

---

M S Murali Murugavel

A Dissertation

Submitted to the Faculty

of the

WORCESTER POLYTECHNIC INSTITUTE

in partial fulfillment of the requirements for the

Degree of Doctor of Philosophy

in

Mechanical Engineering

May 2009

APPROVED:

---

Professor John M. Sullivan, Jr.  
Advisor

---

Professor Matthew O. Ward  
Committee Member

---

Professor Brian J. Savilonis  
Committee Member

---

Professor Gregory S. Fischer  
Committee Member

---

Professor Mark W. Richman  
Graduate Committee Representative

## Abstract

The Pulse Couple Neural Network (PCNN) was developed by Eckhorn to model the observed synchronization of neural assemblies in the visual cortex of small mammals such as a cat. In this dissertation, three novel PCNN based automatic segmentation algorithms were developed to segment Magnetic Resonance Imaging (MRI) data: (a) PCNN image 'signature' based single region cropping; (b) PCNN – Kittler Illingworth minimum error thresholding and (c) PCNN – Gaussian Mixture Model – Expectation Maximization (GMM-EM) based multiple material segmentation. Among other control tests, the proposed algorithms were tested on three T2 weighted acquisition configurations comprising a total of 42 rat brain volumes, 20 T1 weighted MR human brain volumes from Harvard's Internet Brain Segmentation Repository and 5 human MR breast volumes. The results were compared against manually segmented gold standards, Brain Extraction Tool (BET) V2.1 results, published results and single threshold methods. The Jaccard similarity index was used for numerical evaluation of the proposed algorithms. Our quantitative results demonstrate conclusively that PCNN based multiple material segmentation strategies can approach a human eye's intensity delineation capability in grayscale image segmentation tasks.

**Keywords:** PCNN, brain cropping, small mammals, neural networks, segmentation, brain segmentation, GM-WM-CSF, breast cropping, adipose-fibroglandular tissue.

## Acknowledgement

1. Overall: This dissertation was made possible simply because of the support, endless patience, persistence and guidance of my parents and my advisor John M. Sullivan, Jr. Outliers of this cluster include my sister, chithi and chithappa.
2. Dissertation document: I wish to record my thanks to the committee members, Matthew O. Ward (+ computer vision class and queries), Brian J. Saviolis (+ general support), Mark W. Richman (+ general support, TA) and Gregory S. Fischer for agreeing to be on board.
3. Brain atlas work: Praveen Kulkarni, Hamid Ghadyani, Sasidhar Tadanki, Gene Bogdanov, Wei Huang, Aghogho Obi, Anil Kumar Patro.
4. MIVA: Udo Benz, James Zhang.
5. fMRI statistics: Craig Ferris, Marcelo Febo, Karl Schmidt, Karl Helmer, Joseph Petrucelli, Stephen Baker, Steven Bird, Jayson Wilbur.
6. Nerve cell experiment: Dan Gibson, Ryan Marinis, Cosme Furlong, Elizabeth Ryder, Peter Hefti.
7. MR breast segmentation: Subhadra Srinivasan, Adam J Pattison, Colin Carpenter, Keith Paulsen, Robert Ludwig.
8. Remote assistance: Adam J Schwarz, Shawn Mikula, Ghassan Hamarneh, Jason Kinser, Vlatko Becanovic, Thomas Lindblad, Hanbing Lu, Elliot A. Stein, Marc Raichle, Marius Schamschula, Matthew McAuliffe, Nancy J. Lobaugh, Prashanth Udupa, Saulius Garalevicius, Hang Si, B. Sankur.

9. Other projects: Adriana Hera, Christopher Sotak, Mathew Brevard, Govind Bhagavatheeshwaran, Gordon Library (journal articles and ILL division staff), Wei Chen, Shivin Misra, Carolina Ruiz, Ted Clancy, William D Hobey.
  
10. Computer related: CCC Helpdesk, Siamak Najafi, Bob Brown, Randolph Robinson.
  
11. Financial: WPI ME Department (Major), this work was supported in part by NIH P01CA080139-08, WPI GSG and Frontiers.
  
12. Related support, courses, TA: Mohanasundaram, Nandhini, Ganesh, Chirag, Siju, Souvik, Barbara Edilberti, Barbara Furhman, Pam St. Louis, Wayne Zarycki, Lawrence Riley, Marlene, SP, Gana, Janice Martin, Billy McGowan, Tom Thomsen, Allen Hoffman, Michael Demetriou, Zhikun Hou, Mikhail Dimentberg, David Olinger, Hartley Grandin, John Hall, Joseph Rencis.

## Table of Contents

<b>List of Figures</b>	iii
<b>List of Tables</b>	v
<b>1. Introduction</b>	
1.1 Medical imaging modalities	01
1.2 Magnetic Resonance Imaging (MRI) segmentation	02
1.3 Pulse Coupled Neural Network (PCNN)	03
1.4 Outline	04
<b>2. Automatic Cropping of MRI Rat Brain Volumes using Pulse Coupled Neural Networks</b>	
2.1 Introduction	07
2.2 Materials and Methods	11
2.2.1 Overview	11
2.2.2 The PCNN formulation	18
2.2.3 Morphological, contour operations on accumulated PCNN iterations	22
2.2.4 Traditional ANN based selection of brain mask	23
2.3 Experiment details and description	24
2.3.1 Data	24
2.3.2 Parameters employed	27
2.4 Discussion	30
2.4.1 Results	30
2.4.2 Alternate PCNN iteration selection strategies	34
2.5 Conclusion	35
2.6 Supplementary Material	36
<b>3. Multiple region segmentation using a PCNN</b>	
3.1 Introduction	37
3.2 Materials and Methods	41
3.2.1 The Eckhorn Pulse Coupled Neural Network	41
3.2.2 Minimum Error Thresholding	44
3.2.3 1D ' <i>Time signature</i> ' representation of multi region segmentation	45
3.2.4 ANN based selection	48
3.2.5 Gaussian Mixture Model (GMM) based selection	51
3.3 Experiment details	52
3.3.1 Data	52
3.3.2 Parameters employed in the ANN based selection method	52
3.3.3 Parameters employed in the GMM – EM based selection method	53
3.4 Results and Discussion	57
3.4.1 Results	57
3.4.2 Discussion	62

3.5 Conclusions	64
3.6 Supplementary Material	64
<b>4. Automatic cropping and segmentation of MRI breast volumes using Pulse Coupled Neural Networks</b>	
4.1 Introduction	66
4.2 Materials and Methods	68
4.2.1 Overview	68
4.2.2 The Eckhorn Pulse Coupled Neural Network	78
4.2.3 Morphological, contour operations on accumulated PCNN iterations	80
4.2.4 Traditional ANN based selection of breast mask	82
4.2.5 Minimum Error Thresholding	83
4.2.6 Gaussian Mixture Model (GMM) based selection	85
4.3 Experiment details	86
4.3.1 Data	86
4.3.2 Software specifications	87
4.3.3 Parameters employed in the ANN based cropping scheme	87
4.3.4 Parameters employed in the PCNN minimum error thresholding method	90
4.3.5 Parameters employed in the GMM – EM based selection method	92
4.4 Results and Discussion	
4.4.1 Breast cropping results	94
4.4.2 Adipose and Fibroglandular tissue segmentation results	95
4.5 Conclusion	97
<b>5. Conclusions and Future Work</b>	98
<b>References</b>	103

## List of Figures

2.1	Schematic of a multiple slice volume of a rat brain. The highlighted slice has been intensity rescaled [0 1].	13
2.2	Subfigures (a) – (f) illustrate the raw binary PCNN iteration numbers 10, 20, 25, 30, 40 and 50 respectively of the highlighted coronal grayscale slice of Figure 2.1.	14
2.3	The center sub-figure is a close-up of the highlighted region on the left. The right sub-figure illustrates the result of the applied morphological operation meant to break small bridges that connect the brain tissue with the skull.	14
2.4	Subfigures (a) – (f) illustrate the largest contiguous region of PCNN iteration numbers 10, 20, 25, 30, 40 and 50 respectively of the highlighted coronal grayscale slice of Figure 2.1 after the morphological operation.	15
2.5	The predicted PCNN iteration (highlighted) is presented with an override option and alternate choices.	16
2.6	Illustrates the characteristic shape of the normalized image signature G.	17
2.7	Full 3D representation of the cropped brain with end overlaid by corresponding 2D cropped grayscale slice.	18
2.8	The 3 columns (L to R) represent the contours of the brain mask predicted by BET (Jaccard index 0.84), Manual gold standard (Jaccard index 1.0) and the Automatic PCNN (Jaccard index 0.95) overlaid on the corresponding anatomy image.	33
3.1	Subfigure (a) is a sample cropped grayscale slice from the IBSR volume 1_24. Subfigures (b)-(f) illustrate the raw, accumulated <i>binary</i> PCNN iterations 5,10,15,20 and 110 respectively.	39
3.2	Subfigure (a) illustrates a 3D surface mesh (Ziji Wu 2003) of the rat brain overlaid with 3 cropped grayscale slices. Subfigures (b) – (d) illustrate the brain masks obtained using the automatic PCNN algorithm (Murugavel and Sullivan Jr. 2009a).	40
3.3	Illustrates the adaptation of the Kittler Illingworth (1986) method to segment multiple regions on a simulated dataset. Figure 3(a) shows a 3 region grayscale image corrupted with noise (SNR = 15) (source: IBSR simulated data). Figure 3.3(b) is a plot of the computed PCNN Kittler – Illingworth time measure for 3 regions against the corresponding accumulated PCNN iterations. Figure 3.3(c) shows the accumulated pulse 102, which corresponds to the minimum of the time series representation in Figure 3.3(b).	47
3.4	Subfigures (a)-(f) illustrate the raw, accumulated PCNN iterations 3, 13, 50, 54, 148 and 242 of the grayscale slice illustrated in Figure 3.1(a).	49
3.5	Plot of the computed PCNN Kittler – Illingworth time measure for 2 regions against the corresponding accumulated PCNN iterations.	50

3.6	Allows for qualitative comparison of the performance of the PCNN ANN and the PCNN – GMM EM algorithms. Rows (a) through (c) span the brain spatially. The two extreme columns show segmentation results from the PCNN ANN and PCNN – GMM EM algorithms, respectively. The middle column shows the corresponding manual mask obtained from IBSR.	58
4.1	Subfigures (a) – (c) show coronal, sagittal and transverse sections of a breast volume. The serrated pattern observed on the periphery was caused by the transducer arrays positioned required by the alternate breast imaging modalities such as NIS described in Section 4.1. The adipose tissue is generally of a higher intensity, while the darker irregular pattern constitutes fibroglandular tissue.	70
4.2	Subfigures (a) – (e) illustrate the raw, accumulated binary PCNN iteration numbers 5, 10, 15, 20, 30 and 40 respectively of the coronal grayscale slice of Figure 4.1(a).	71
4.3	Subfigures (L-R) show respectively, the accumulated PCNN iteration number 27 of the grayscale slice of Figure 4.1(a), detail of unbroken bridges highlighted in left figure before application of the morphological operator and detail after the application of the morphological operator.	72
4.4	Subfigures (a) – (e) illustrate, the morphologically processed; largest enclosed contiguous areas. The morphological operator serves to break small slivers that might connect transducer array artifacts to the breast tissue in a few early iterations.	73
4.5	The ANN based prediction (highlighted) with manual over ride option.	74
4.6	Illustrates the characteristic shape of the normalized image signature $G$ . The task is to simply identify a PCNN iteration close to the beginning of the plateau region.	75
4.7	3D surface mesh of the breast volume shown in Figure 4.1 with inlays of 2 sample coronal grayscale slices. The mesh was generated via the Multiple Material Marching Cubes (M3C) algorithm described by Wu and Sullivan (2003).	76
4.8	Qualitative results of two region segmentation algorithms on 2D slices identified by ‘1907_40’ and ‘506_32’ (Table 4.6) in columns. Figures in rows, illustrate results of manual PCNN selection (‘Gold’ standard), PCNN-Kittler, PCNN GMM-EM and Kittler-Illingworth thresholding algorithms. The red colored region marks adipose tissue, while the green color region encodes fibroglandular tissue.	77

## List of Tables

1.1	Current medical imaging modalities and their EM spectrum range	2
2.1	The values of the PCNN coefficients used in this algorithm were sourced from Johnson and Padgett (1999) and Waldemark et al. (2000).	21
2.2	Pseudo code of rat brain cropping algorithm	29
2.3	Lists the performance metrics of the automatic PCNN, BET V2.1 on the three different datasets described in the paper.	32
3.1	The values of the PCNN coefficients used in this algorithm were sourced from Johnson and Padgett (1999) and Waldemark, et al. (2000).	43
3.2	Pseudo code of PCNN – ANN based selection method	55
3.3	Pseudo code of PCNN – GMM EM based selection method	56
3.4	Jaccard indices obtained on each subject of the IBSR database for each class. Indices are presented for both the PCNN - ANN selection and the PCNN - GMM EM selection strategies.	60
3.5	Comprehensive comparison of published average Jaccard indices on the 20 T1 weighted volumes available at IBSR.	61
4.1	The values of the PCNN coefficients used in this algorithm were sourced from Johnson and Padgett (1999) and Waldemark, et al. (2000).	80
4.2	Pseudo code of the automatic breast cropping algorithm	89
4.3	Pseudo code of PCNN - Minimum Error Thresholding based selection method	91
4.4	Pseudo code of PCNN – GMM EM based selection method	93
4.5	Jaccard indices obtained on five breast volumes employing the PCNN based cropping method.	96
4.6	Jaccard indices obtained on the 10 breast slices employed in evaluation of the PCNN minimum error thresholding, PCNN GMM – EM based formulation and the standard Kittler Illingworth (single threshold) method.	97

# Chapter 1

## Introduction

### 1.1 Medical imaging modalities

The discovery of X-rays (1895) by the subsequent Nobel prize winner (1901), Wilhelm Roentgen led to the first medical image based diagnosis by Dr. Hall Edwards (1896). Since then different parts of the Electro Magnetic (EM) spectrum have been exploited for medical imaging. In economic terms the United States medical imaging market is estimated to be worth \$11.4 billion by 2012 (BCC Research, Medical Imaging: Equipment and Related Products).

A recent (2003) Nobel prize (Paul C Lauterbur and Peter Mansfield) recognized the discovery of Magnetic Resonance Imaging (MRI) in the early 1970s. See Keller (1988) for a detailed description of MR imaging modality.

Table 1.1 (adapted from Demirkaya et al., 2009) lists the various common medical imaging modalities, the EM spectrum range and the corresponding photon energy involved. MRI, owing to its lower energy dosage and excellent soft tissue imaging capabilities has witnessed rapid adoption as a medical diagnosis tool. In 2002 alone, there were more than 60 million MRI examinations performed ([http://nobelprize.org/nobel\\_prizes/medicine/laureates/2003/press.html](http://nobelprize.org/nobel_prizes/medicine/laureates/2003/press.html)).

Further, the MR modality is being fielded in areas such as surgery (Interventional MRI), radiation therapy simulation: to locate and mark tumors, functional MRI: a measure of the BOLD (Blood Oxygen Level Dependent) signal and MR Elastography (MRE) (Paulsen et al., 2005). Each of these applications has resulted in increased need of automatic MR segmentation algorithms. Another quantitative metric that highlights the tremendous research interest in this field is reflected by a search on Google scholar for the keyword 'mri segmentation'. In April 2009, this search yielded 93,300 possible matches.

<b>Imaging modality</b>	<b>Energy range (eV)</b>	<b>Frequency range (Hz)</b>
MRI	$1.654 \times 10^{-7} - 2.068 \times 10^{-7}$	$40 \times 10^6 - 50 \times 10^6$
Light microscopy, Fluorescence imaging	1.77 - 3.09	$4.28 \times 10^{14} - 7.49 \times 10^{14}$
X-ray (Radiograph, Computerized Tomography, Mammography)	20000 - 200000	$4.8 \times 10^{18} - 4.8 \times 10^{19}$
Low energy gamma rays (Single Photon Emission Tomography)	60000 - 300000	$1.45 \times 10^{19} - 7.25 \times 10^{19}$
High energy gamma rays (Positron Emission Tomography)	511000	$1.23 \times 10^{20}$

**Table 1.1:** Current medical imaging modalities and their EM spectrum range

## 1.2 Magnetic Resonance Imaging (MRI) segmentation

Current automatic segmentation algorithms (Pham, et al. 2000) are usually clustered into the one of the following classes: Thresholding (Mikheev, et al. 2008; Schnack, et al. 2001), Classifier based (Ashburner and Friston 2005), Markov

Random Field Models (Rivera, et al. 2007), Artificial Neural Networks (ANN) (Reddick, et al. 1997), deformable surface based (Zhuang, et al. 2006) and hybrid methods (Ségonne, et al. 2004). It must be noted that almost all traditional segmentation methods lack an actual understanding of the image. See Hawkins and Blakeslee (2008) for a general treatment of this idea. However, there has been a sustained interest in ANN and pattern recognition methods (Egmont-Petersen, et al. 2002) for automatic segmentation of MR images.

A few researchers such as Belardinelli, et al. (2003) have attempted to use a neural network model that simulates the functionality of the human visual cortex in which each pixel is mapped to an individual oscillator to effect segmentation of MR images. In this dissertation, a similar '*biomimetic*' segmentation method known as the Pulse Coupled Neural Network (PCNN) is employed for automatic segmentation of MR data.

### **1.3 Pulse Coupled Neural Network (PCNN)**

The PCNN is based on neurophysiological studies of the primary visual cortex of a cat by Eckhorn et al.(1990). They developed a neural network model which captured the observed global linking of cell assemblies as a result of feature similarity in sensory systems. The specific algorithm used in this dissertation is the Eckhorn model implemented by Johnson and Padgett (1999) and Waldemark et al. (2000). The segmentation is accomplished using the feature extraction property that Eckhorn et al. (1990) described in the 'Linking' part of their neural network model,

which associates regions of input images that are similar in intensity and texture. Lindblad and Kinser (2005) cover numerous aspects of the PCNN model tuned for image processing applications. Several independent research groups have applied the basic Eckhorn model for various applications; image segmentation (Kuntimad and Ranganath 1999), image thinning (Gu, et al. 2004) and path optimization (Caulfield and Kinser 1999). A recent pattern recognition procedure (Muresan 2003) involved the use of the PCNN to generate a 1D time signature from an image. This time signature was then trained using a back propagation neural network model for image recognition. A similar idea is employed in this dissertation to effect multiple region image segmentation as opposed to image recognition.

#### **1.4 Outline**

The remainder of this dissertation is organized as three separate, self contained chapters containing material sourced from published manuscripts or material in advanced stage of preparation.

In Chapter two, we show the use of the PCNN as an image segmentation strategy to crop MR images of rat brain volumes. We then show the use of the associated PCNN image 'signature' to automate the brain cropping process with a trained artificial neural network. We tested this novel algorithm on three T2 weighted acquisition configurations comprising a total of 42 rat brain volumes. The datasets included 40 ms, 48 ms and 53 ms effective TEs, acquisition field strengths of 4.7T and 9.4T, image resolutions from 64x64 to 256x256, slice locations ranging from +6

mm to -11 mm AP, two different surface coil manufacturers and imaging protocols. The results were compared against manually segmented gold standards and Brain Extraction Tool (BET) V2.1 results. The Jaccard similarity index was used for numerical evaluation of the proposed algorithm. Our novel PCNN cropping system averaged 0.93 compared to BET scores circa 0.84.

Variations in intensity distribution are a critical feature exploited in manual segmentation of images. In Chapter three, we describe two novel algorithms that employ a PCNN model to segment T1 weighted MRI human brain data into its constituent classes, Grey Matter (GM), White Matter (WM) and Cerebro-Spinal Fluid (CSF). The first technique employs a modified version of the Kittler and Illingworth thresholding method to generate a surrogate time signature of the accumulated PCNN iterations. We describe the use of this time signature to segment simulated and real data from the Harvard Internet Brain Segmentation Repository. The Jaccard index returned averages of 0.72 and 0.61 for the GM and WM respectively for the 19 T1 weighted MRI brain volumes. The second technique estimates the composition of each grayscale image slice via a Gaussian Mixture Model (GMM) Expectation Maximization (EM) formulation. A feature vector of the estimated means, standard deviations and composition proportions was then assembled and compared against the corresponding computed measure of individual, accumulated PCNN iterations to determine the best segmentation match. This unsupervised approach returned Jaccard index averages of 0.76, 0.66 and 0.13 for the GM, WM and CSF respectively for the 20 T1 weighted MRI brain volumes. These data compare to

Jaccard index averages of 0.88 (GM), 0.83 (WM) for manual segmentations of 4 brain volumes averaged over two experts and 0.61 (GM), 0.62 (WM), 0.09 (CSF) for the average of a dozen other segmentation strategies in use.

In Chapter four we describe the PCNN as a unified tool to automatically crop and segment human breast MR volumes into adipose and fibroglandular regions. Each 2D constitutive grayscale MR slice is represented as a 1D time signature generated via the PCNN iterating in an *'accumulate'* configuration. A Multi Layer Perceptron (MLP) classifier was then trained to automatically crop breast tissue from the surrounding air and transducer artifacts. Adipose and fibroglandular segmentation was effected on the cropped 2D slices by two unsupervised methods; minimization of a PCNN based Kittler-Illingworth formulation and a PCNN – Gaussian Mixture Model algorithm. The proposed automatic cropping algorithm was tested on 5 MR breast volumes consisting of 248 slices (256 x 256). The results were compared against manual selections obtained via the PCNN. The resulting Jaccard index mean of 0.99 indicates a highly successful outcome of the method. The effectiveness of the proposed adipose – fibroglandular segmentation strategies were tested using 10 cropped grayscale slices and corresponding manual PCNN segmentation selections. For control, the Kittler-Illingworth thresholding method was employed. The mean Jaccard indices for the adipose – fibroglandular regions were 0.78, 0.94 (PCNN-Kittler Illingworth formulation), 0.78, 0.92 (PCNN – GMM) and 0.49, 0.86 (Kittler Illingworth thresholding).

Conclusions and future work directions can be found in Chapter five.

## Chapter 2

# Automatic Cropping of MRI Rat Brain Volumes using Pulse Coupled Neural Networks

### 2.1 Introduction:

A common precursor to several neuroimaging analyses is the use of Brain Extraction Algorithms (BEAs) designed to crop brain tissue from non brain tissues such as cranium, eyes, muscles and skin. Following a BEA application, also described as intracranial segmentation or skull stripping, several downstream and independent applications are applied, such as registration of subjects to an atlas for Region Of Interest (ROI) analysis (Grachev et al., 1999), brain tissue segmentation (Shattuck et al., 2001), functional Magnetic Resonance Imaging (fMRI) analysis preprocessing (Beckmann et al., 2006) and monitoring brain volume as a function of time to study brain atrophy (Battaglini et al., 2008). Although these researchers applied BEA and subsequent neuroimaging techniques on human subjects, the number of neuroimaging studies on animal models such as the rat is growing rapidly, providing new insights into brain function as well as improved translation to/from analogous clinical studies. Schwarz et al. (2006) cropped 97 brain volumes in the development of a stereotaxic Magnetic Resonance Imaging (MRI) template for the rat brain. The processing pipeline of the somatosensory pathway mapping fMRI study of Lowe et al. (2007), the pharmacological fMRI study of Littlewood et al. (2006) included rat brain cropping. Ferris et al. (2005) registered rat brain volumes to an atlas for ROI analysis. Yet, an efficient brain cropping algorithm focused on small mammals is lacking.

Automated brain extraction is a subset (Smith, 2002; Zhuang et al., 2006), of general image segmentation strategies which delineates edges between regions frequently exhibiting similar texture and intensity characteristics. However, there is no definitive line separating extraction (cropping) and segmentation functions. All published automated BEAs use various combinations of basic segmentation (Pham et al., 2000) techniques on individual slices or on entire 3D volumes to crop brain tissue from non brain tissue. Frequently (Smith, 2002; Ségonne et al., 2004), automated BEAs have been clustered into the following broad classes: thresholding with morphology based methods (Lee et al., 1998; Lemieux et al., 1999; Mikheev et al., 2008), deformable surface based (Aboutanos et al., 1999; Dale et al., 1999; Kelemen et al., 1999; Smith, 2002; Zhuang et al., 2006) and hybrid methods (Rehm et al., 2004; Rex et al., 2004; Ségonne et al., 2004) . Each of these methodologies have advantages and all areas are being advanced. There is clear evidence (Lee et al., 2003; Rex et al., 2004; Fennema-Notestine et al., 2006; Zhuang et al., 2006) that no single BEA is suitable for all studies or image acquisition protocols. Generally, human intervention is employed for satisfactory cropping.

Our review of automated BEAs noted a fundamental lack of these algorithms applied to small animals. The methodology has been applied dominantly on human subjects. Most brain tissue cropping in small laboratory animals continues to be manual or semi automatic (Pfefferbaum et al., 2004; Wagenknecht et al., 2006; Sharief et al., 2008). Some studies such as Schwarz et al. (2006) working with T2 weighted Rapid Acquisition with Relaxation Enhancement (RARE) sequences have

successfully used semi automatic segmentation tools (Kovacevic et al., 2002) developed for the human brain in animal models. Kovacevic et al. (2002) had reported a histogram based technique involving the use of co registered Proton Density (PD), T2 weighted anatomy data to crop T1 weighted anatomy images of the human brain. This idea has been supported by the skull and scalp stripping work of Dogdas et al. (2005) and Wolters et al. (2002) who establish that the inner skull boundary can be determined more accurately by the use of PD images. Another example Roberts et al. (2006) uses an adaptation of Brain Extraction Tool (BET) (Smith, 2002) with manual correction for extraction of the rat brain from RARE anatomy data. However, the overall quality of the small animal brain extraction is significantly lower than that obtained for human images (FSL).

This article presents a novel Pulse Coupled Neural Network based approach to automatically crop rat brain tissue. The proposed method takes advantage of the specificity accorded by T2 weighted images in terms of contrast for the proton rich brain environment and the inherent segmentation characteristics of the PCNN to rapidly crop the rat brain. The method described here does not attempt a second level segmentation to differentiate, for instance, White matter from Grey matter. Rather, the focus is to crop the brain quickly and automatically so that subsequent operations, such as registration can proceed immediately.

Artificial Neural Network (ANN) and Pattern Recognition methods (Egmont-Petersen et al., 2002) have been widely applied on the brain tissue type segmentation

problem (Reddick et al., 1997; Dyrby et al., 2008; Powell et al., 2008). However, there have been very few neural network approaches that specifically address the problem of automatic brain extraction. Congorto et al. (1996) used a Kohonen Self Organizing Map approach which combines self-organization with topographic mapping and classifies image regions by similarities in luminance and texture. They applied this technique on 2 dimensional T1 slices to segment the image into 3 classes: scalp, brain and skull. Belardinelli et al. (2003) used an adaption of a LEGION (Locally Excitatory Globally Inhibitory Network) for segmenting T1 weighted 2D images. The LEGION is a neural network model that simulates the human visual cortex in which each pixel is mapped to an individual oscillator and the size of the network is the same as that of the input image. Both Congorto et al. (1996) and Belardinelli et al. (2003) provided qualitative results but did not report extensive testing of their respective algorithms on large datasets.

The underlying algorithm used in this paper is the standard Eckhorn PCNN model (Johnson and Padgett, 1999). The PCNN is a neural network model based on the visual cortex of a cat, which captures the inherent spiking nature of the biological neurons. The brain extraction is accomplished using the feature extraction property that (Eckhorn et al., 1990), described in the 'Linking' part of their neural network model, which associates regions of input images that are similar in intensity and texture. Lindblad and Kinser (2005) cover numerous aspects of the PCNN model tuned for image processing applications. Several independent research groups have applied the basic Eckhorn model for various applications; image segmentation

(Kuntimad and Ranganath, 1999), image thinning (Gu et al., 2004) and path optimization (Caulfield and Kinser, 1999). A recent pattern recognition procedure (Muresan, 2003) involved the use of the PCNN to generate a 1D time signature from an image. This time signature was then trained using a back propagation neural network model for image recognition. The method proposed in this article follows a similar approach.

## **2.2 Materials and Methods**

### **2.2.1 Overview**

The proposed brain extraction algorithm operates on individual 2D grayscale data (slices), Figure 2.1. For purposes of illustration of the proposed algorithm we follow the various operations on the representative 2D slice highlighted in Figure 2.1. Intensity rescaling to [0 1] is the first operation on each 2D slice, as noted on the highlighted slice in Figure 2.1. The PCNN algorithm is then applied in the 'accumulate' mode (discussed subsequently) on individual 2D slices, Figure 2.2. A morphological operator is employed to break 'narrow bridges' that might link the brain tissue with other regions, like the skull, Figure 2.3. A contour operation is used with level set to unity. Only the largest contiguous region from each PCNN iteration is selected, Figure 2.4. The contour outlines corresponding to the selected regions are then overlaid on the corresponding grayscale image, Figure 2.5. At this stage the problem is rendered to one of choosing a particular iteration that best outlines the

brain region. The accumulated response as a function of iteration has a characteristic behavior as shown in, Figure 2.6. Several techniques can be used to identify the first plateau in Figure 2.6. A previously trained ANN can be used to identify the iteration that best represents the brain outline. In this mode, one has the option to view the predicted selection with override ability, Figure 2.5. This process is repeated for each slice resulting in a set of mask slices that can be used in a marching cube routine (Wu and Sullivan, 2003) to create a full 3D geometry representation of the cropped brain, Figure 2.7.



**Figure 2.1.** Schematic of a multiple slice volume of a rat brain. The highlighted slice has been intensity rescaled [0 1].

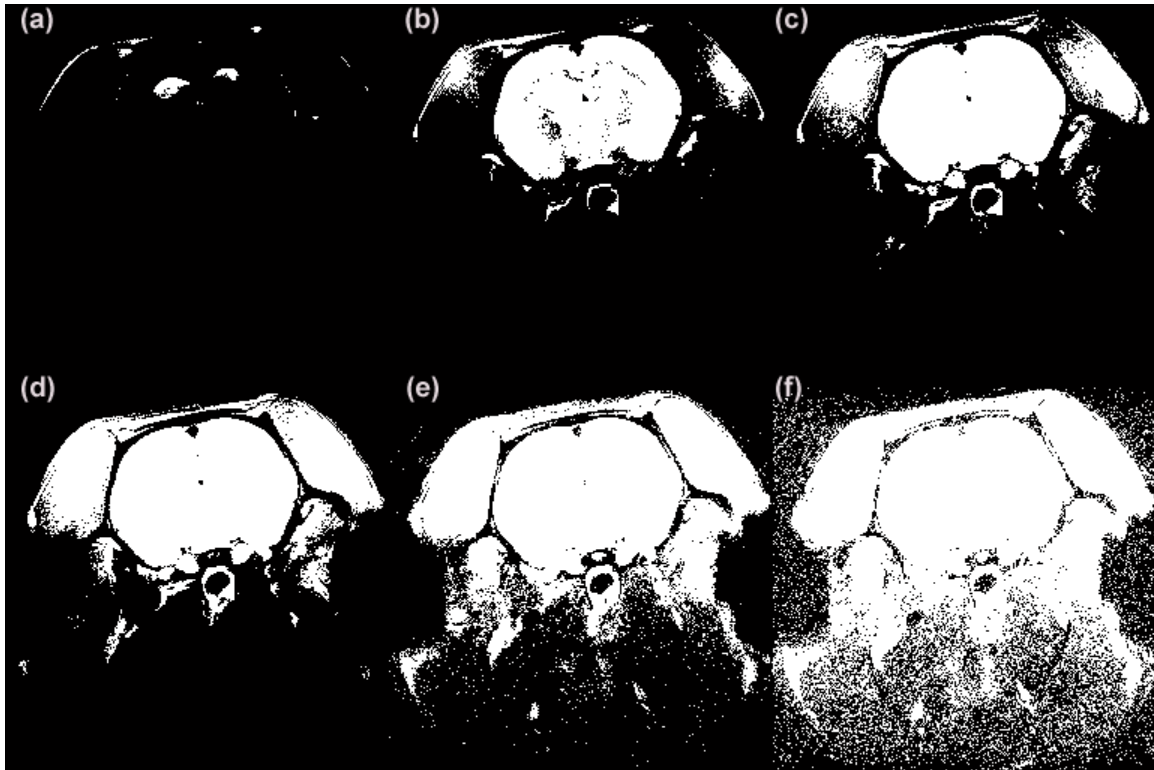


**Figure 2.2.** Subfigures (a) – (f) illustrate the raw binary PCNN iteration numbers 10, 20, 25, 30, 40 and 50 respectively of the highlighted coronal grayscale slice of Figure 2.1.

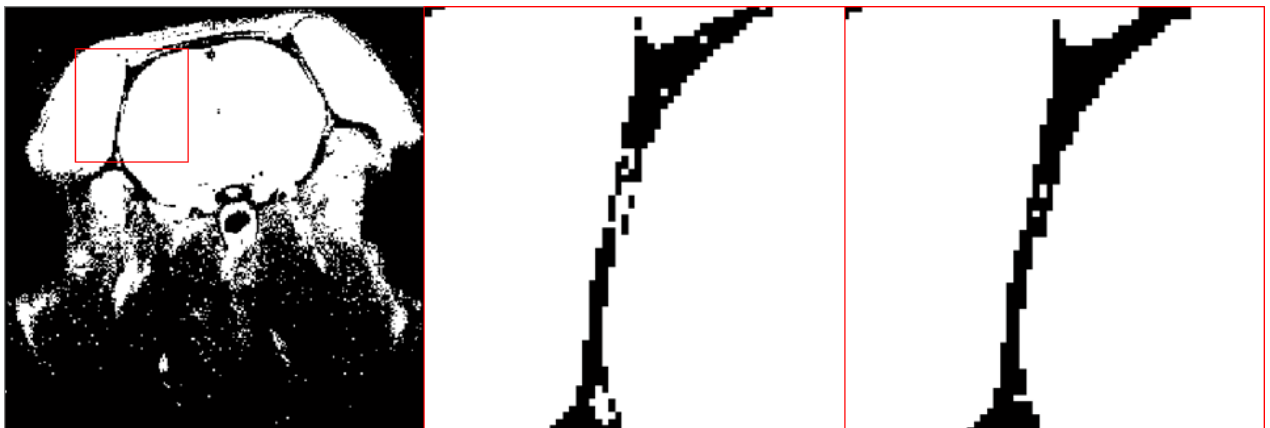


**Figure 2.3.** The center sub-figure is a close-up of the highlighted region on the left. The right sub-figure illustrates the result of the applied morphological operation meant to break small bridges that connect the brain tissue with the skull.

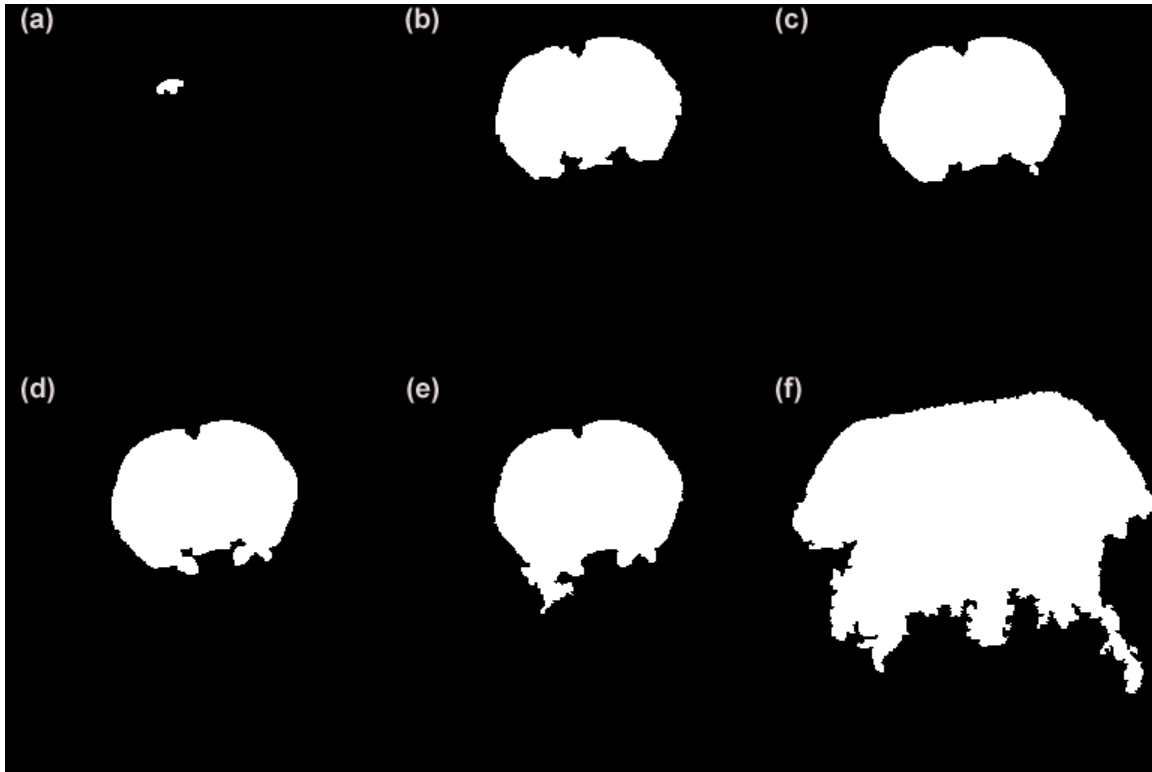


**Figure 2.4.** Subfigures (a) – (f) illustrate the largest contiguous region of PCNN iteration numbers 10, 20, 25, 30, 40 and 50 respectively of the highlighted coronal grayscale slice of Figure 2.1 after the morphological operation.

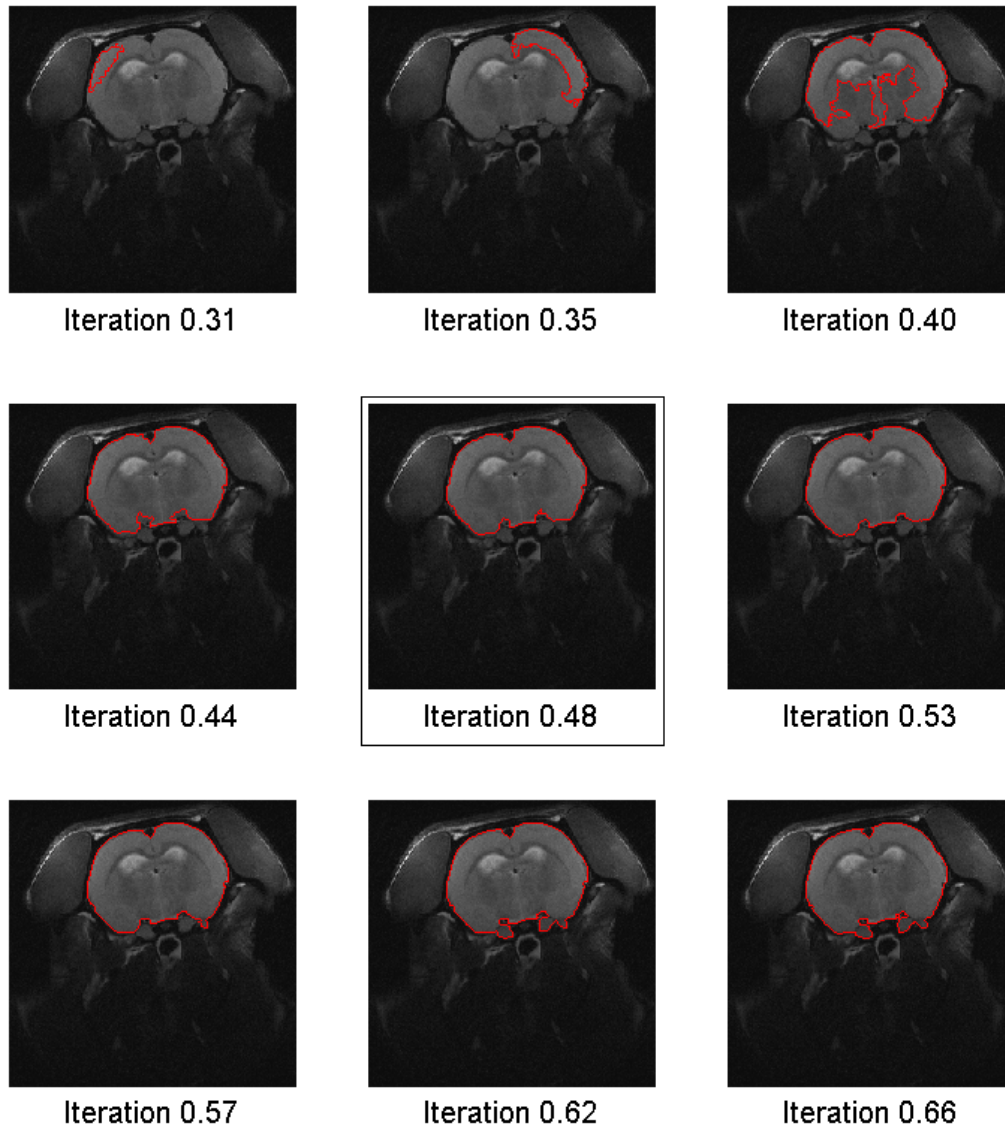


**Figure 2.5.** The predicted PCNN iteration (highlighted) is presented with an override option and alternate choices.

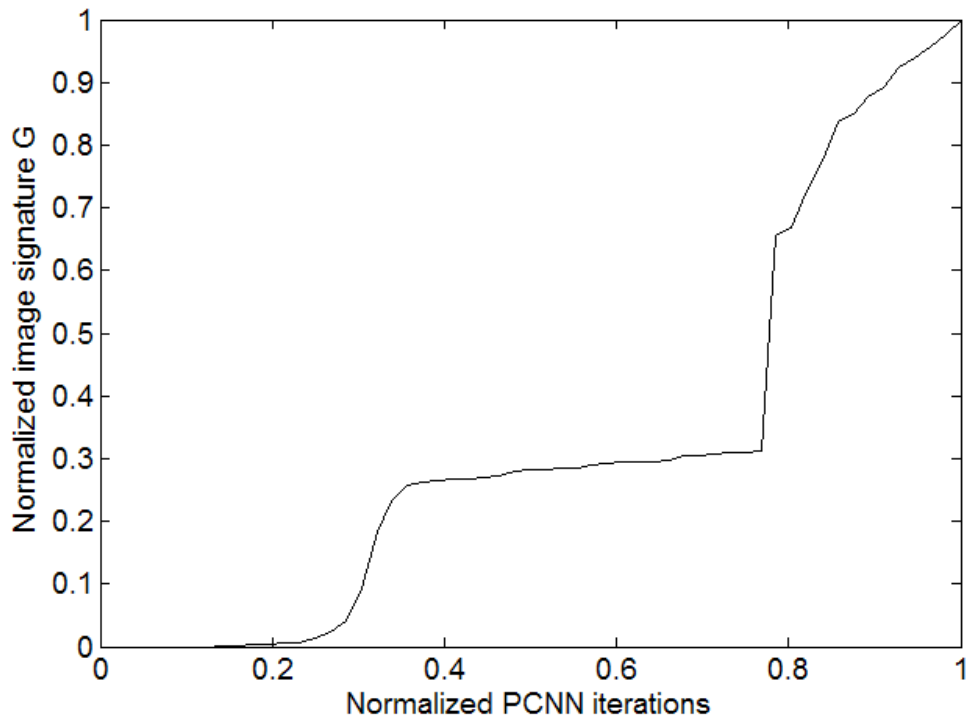


**Figure 2.6.** Illustrates the characteristic shape of the normalized image signature  $G$ .

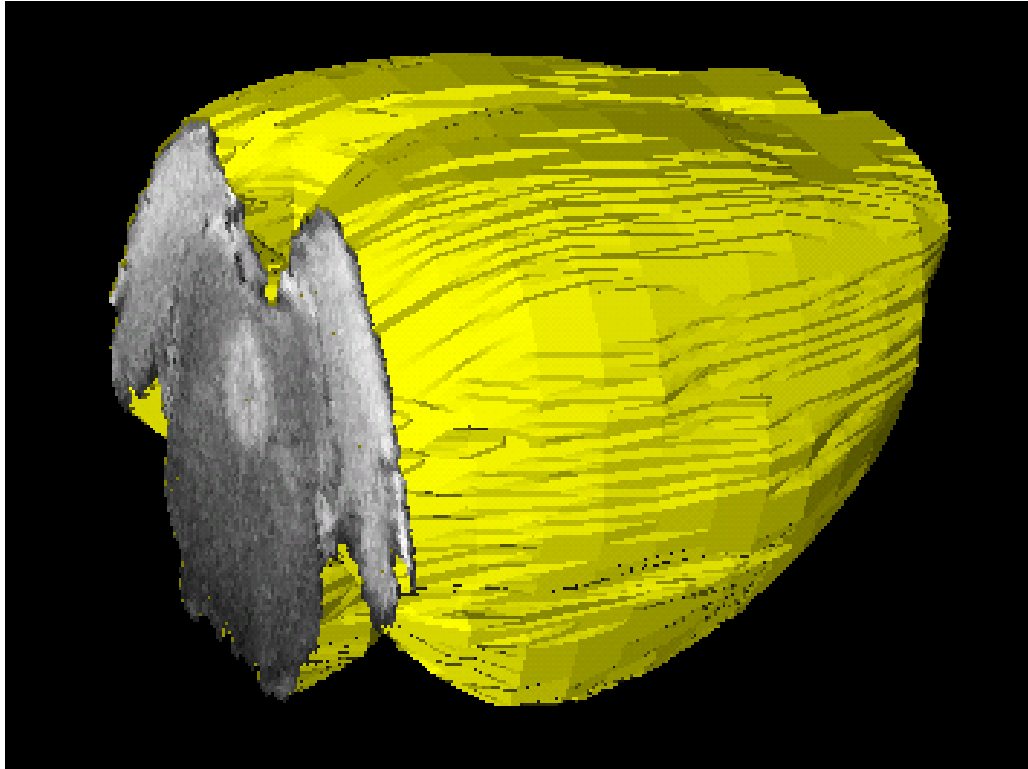


**Figure 2.7.** Full 3D representation of the cropped brain with end overlaid by corresponding 2D cropped grayscale slice.

### **2.2.2 The PCNN Formulation:**

The PCNN belongs to a unique category of neural networks, in that it requires no training (Lindblad and Kinser, 2005) unlike traditional models where weights may require updating for processing new inputs. Specific values (Table 2.1) of the PCNN coefficients used in our work were derived from Johnson and Padgett (1999) and Waldemark et al. (2000).

Generally, a 3D volume of grayscale coronal slices of the rat brain is created in the MR system. Since the PCNN operates on 2D data, individual slices are sequentially extracted and their grayscale intensities normalized within the range [0, 1].

Let  $S_{ij}$  be the input grayscale image matrix. The subscripts  $i, j$  denote the position of the PCNN ‘neuron’ as well as the corresponding pixel location of the input grayscale image. Each neuron in the processing layer of the PCNN is coupled directly to an input grayscale image pixel or to a set of neighboring input pixels with a predefined radius  $r$ . Functionally, it consists of a Feeding and Linking compartment, described by arrays  $F_{ij}$  and  $L_{ij}$ , each of dimension equaling the 2D input grayscale image, linked by two synaptic weighting matrices  $M$  and  $W$ . The synaptic weighting matrix is square with a dimension of  $(2r + 1)$  and is a normalized Gaussian about the center of the square matrix.

$$F_{ij}[n] = e^{-\alpha_F} F_{ij}[n-1] + S_{ij} + V_F (M * Y[n-1])_{ij} \quad (2.1)$$

$$L_{ij}[n] = e^{-\alpha_L} L_{ij}[n-1] + V_L (W * Y[n-1])_{ij} \quad (2.2)$$

$$U_{ij}[n] = F_{ij}[n] (1 + \beta L_{ij}[n]) \quad (2.3)$$

$$T_{ij}[n] = e^{-\alpha_T} T_{ij}[n-1] + V_T Y_{ij}[n]$$

(2.4)

$$Y_{ij}[n] = 1 \text{ if } U_{ij}[n] > T_{ij}[n] \quad (2.5)$$

$$Y_{ij}[n] = 0 \text{ if } U_{ij}[n] \leq T_{ij}[n] \quad (2.6)$$

The PCNN is implemented by iterating through equations (2.1)-(2.6) with  $n$  as the current iteration index and ranging from 1 to  $N$  (the total number of iterations). The matrices  $F_{ij}[0], L_{ij}[0], U_{ij}[0]$  and  $Y_{ij}[0]$  were initialized to a zero matrix, while  $T_{ij}[0]$  was initialized to a unit matrix. For each iteration, the internal activation  $U_{ij}$  is computed and compared against the threshold  $T_{ij}$ . Thus, the array  $Y_{ij}[n]$  is a binary image representing the PCNN mask at that particular iteration.

$\alpha_F, \alpha_L, \alpha_T$  are iteration (surrogate time) constants that determine the internal state of the network effecting exponential decay and  $V_F, V_L, V_T$  are magnitude scaling terms for Feeding, Linking and Threshold components of the PCNN.  $*$  is the two dimensional convolution operator.  $\beta$  is a parameter affecting linking strength, Table 2.1.

Constant	PCNN coefficient	Context
$\beta$	0.2	Linking strength
$\tau_F$	0.3	Feeding decay
$\tau_L$	1	Linking decay
$\tau_T$	10	Threshold decay
$V_F$	0.01	Feeding coupling
$V_L$	0.2	Linking coupling
$V_T$	20	Magnitude scaling term for threshold
$r$	3	Radius of linking field

**Table 2.1:** The values of the PCNN coefficients used in this algorithm were sourced from Johnson and Padgett (1999) and Waldemark et al. (2000). Further coefficients  $\alpha_{F,L,T} = \ln 2 / \tau_{F,L,T}$  as described by Waldemark et al. (2000).

Our implementation of the PCNN operates in the ‘accumulate’ mode: that is, each iteration sums its contributions with the previous PCNN iterations.

$$A_{ij}[n] = \sum_{k=1}^n Y_{ij}[k] \quad (2.7)$$

The process described by equation (2.7) can result in a non binary image  $A_{ij}$ . However, for our work the accumulated iteration  $A_{ij}[n]$  is converted into a binary image by means of a thresholding operation at unity, Figure 2.2.

### 2.2.3 Morphological, contour operations on accumulated PCNN iterations

A binary morphological operation breaks 'narrow bridges' or clusters of pixels with a radius less than  $p$  pixels. Each pixel  $i, j$  value (0 or 1) within a PCNN iteration must be continuous in at least two orthogonal directions. That is IF  $(i \pm p, \dots, i \pm 1, i)$  is 1 AND  $(j \pm p, \dots, j \pm 1, j)$  is 1, THEN pixel  $i, j = 1$ .

Perimeters or contours of isolated islands are created. The largest area within each PCNN iteration is selected. All pixels within the selected perimeter are filled with 'ones'. This process results in only one contiguous segment for each PCNN iteration. We denote each PCNN iteration at this stage by  $C_{ij}[n]$  with iteration  $n$  ranging from  $[1, N]$ . Figure 2.4 is used to illustrate the outcome of the described morphological and contour operations on the same coronal section shown in Figure 2.1.

A successful brain extraction results when an appropriate PCNN iteration  $n$  is selected. A 1D time signature is constructed for the PCNN iterations similar to that of

Muresan (2003). The abscissa or timeline is the iteration count. The ordinate is the total number of pixels within the largest contoured area for each PCNN iteration.

$$G[n] = \sum_{ij} C_{ij}[n]$$

Where  $n$  ranges from [1, N]. This image signature has a characteristic shape for similar images with similar regions of interest. This information is used as a surrogate time series in a traditional ANN training sequence to automatically extract the brain tissue. It is also used as the surrogate time in the first order response fitting. The maximum number of iterations (N) of the PCNN is established when the sum of the array  $Y[n]$  (equation (2.6)) exceeds 50% of the image space. This maximum iteration count varies somewhat for each slice and subject. The 50% setting makes the explicit assumption that the region of interest (ROI) occupies less than 50 % of the image space. This variable can be readily set to occupy a higher percentage of the entire image space in the event of the ROI's tending to occupy a larger area.

#### **2.2.4 Traditional ANN based selection of brain mask.**

A previously trained ANN receives the accumulated response as a function of iteration and outputs an iteration number,  $n$ . Multi Layer Perceptron (MLP) is a widely used (Haykin, 1998) supervised, feedforward ANN model which can be trained to map a set of input data to a desired output using standard backpropagation algorithms. Since each grayscale brain coronal section  $S_{ij}$  is now

represented by the PCNN iterations  $C_{ij}[n]$  with  $n$  ranging from  $[1, N]$  and an image signature  $G$ , it is possible to create a training set for the MLP.

Figure 2.6 shows the characteristic shape of the image signature for the sample mid section coronal brain slice. In the illustrated example, iteration numbers corresponding to 0.4 to 0.6 will produce very similar brain masks. This characteristic step response behavior can be fitted easily. It requires few training volumes to create a reliable trained ANN. For the work presented herein, the number of rat brain volumes used to train the network was 7.

The neural architecture of the MLP used in this article consists of one input layer, one hidden layer and a single output neuron. The input layer neurons simply map to the image signature which is a vector of dimension  $N$ . The vector is normalized for the purposes of efficient supervised training using the back propagation algorithm. The hidden layer consisted of about half the number of neurons in the input layer and the single output neuron mapped the desired PCNN iteration corresponding to the brain mask.

## **2.3 Experiment details and description.**

### **2.3.1 Data**

T2 weighted RARE anatomical images (Spenger et al., 2000; Ferris et al., 2005;

Roberts et al., 2006; Schwarz et al., 2006; Canals et al., 2008) are widely used in rat brain studies. Three different coronal datasets representing different imaging field strengths, T2 weightings, resolution and coil manufacturers were assembled to demonstrate the proposed algorithm. The field of view was adjusted to span the entire cranium of the rat. The images were acquired along the coronal section of the rat brain. The data were obtained over multiple imaging sessions and multiple studies.

### **Anatomy dataset (4.7T, 30 volumes)**

The imaging parameters of this dataset are similar to those published by Ferris et al. (2005). Adult Long-Evans rats were purchased from Harlan (Indianapolis, IN, USA) and cared for in accordance with the guidelines published in the Guide for the Care and Use of Laboratory Animals (National Institutes of Health Publications No. 85-23, Revised 1985) and adhere to the National Institutes of Health and the American Association for Laboratory Animal Science guidelines. The protocols used in this study were in compliance with the regulations of the Institutional Animal Care and Use Committee at the University Massachusetts Medical School.

All data volumes were obtained in a Bruker Biospec 4.7 T, 40 cm horizontal magnet (Oxford Instruments, Oxford, U.K.) equipped with a Biospec Bruker console (Bruker, Billerica, MA, U.S.A) and a 20 G/cm magnetic gradient insert (inner diameter, 12 cm; capable of 120  $\mu$ s rise time, Bruker). Radiofrequency signals were sent and

received with dual coil electronics built into the animal restrainer (Ludwig et al., 2004). The volume coil for transmitting RF signal features an 8-element microstrip line configuration in conjunction with an outer copper shield. The arch-shaped geometry of the receiving coil provides excellent coverage and high signal-to-noise ratio. To prevent mutual coil interference, the volume and surface coils were actively tuned and detuned. The imaging protocol was a RARE pulse sequence (Eff TE 48 ms; TR 2100 ms; NEX 6; 7 min acquisition time, field of view 30 mm; 1.2 mm slice thickness;  $256 \times 256 \times 12$  (nrow $\times$ ncol $\times$ nslice) data matrix; 8 RARE factor).

#### **Functional dataset (4.7T, 6 volumes)**

This dataset was obtained with the same hardware and animal specifications as those described in the 4.7 T anatomy dataset. The imaging protocol was a multi-slice fast spin echo sequence (TE 7 ms; Eff TE 53.3 ms; TR 1430 ms; NEX 1; field of view 30 mm; 1.2 mm slice thickness;  $64 \times 64 \times 12$  (nrow $\times$ ncol $\times$ nslice) data matrix; 16 RARE factor). This sequence was repeated 50 times in a 5 minute imaging session of baseline data on 6 different rats. The dataset comprised of MRI functional volumes at the 35<sup>th</sup> time step of the study.

#### **Anatomy dataset (9.4T, 6 volumes)**

The imaging parameters of this dataset are similar to those published by Lu et al. (2007, 2008). The volumes were of a Sprague-Dawley rat, scanned with a Bruker

coil setup, 72 mm volume coil for RF transmission with a 3 cm flat receiver surface coil. The imaging protocol was a RARE sequence (Eff TE 40 ms; TR 2520 ms; field of view 35 mm × 35 mm; 1 mm slice thickness; matrix size 192×192, zero-padded to 256×256 for reconstruction). For the purposes of this study 18 slices from +6 mm to -11 mm AP (Paxinos and Watson 1998) in a coronal plane passing through the Bregma were considered.

### 2.3.2 Parameters employed

The algorithm employing the methods described in Section 2.2 is presented as a pseudo code in Table 2.2. The entire algorithm was implemented in MATLAB 2007b (Mathworks, MA, U.S.A).

The input grayscale brain volumes were treated as the subject data and individually referred to as 'grayscaleAnatomy' variable in Table 2.2. The PCNN algorithm was implemented and the 'PCNNInputParametersVector' of Table 2.2 contained numerical values of the various PCNN parameters,  $\alpha_F, \alpha_L, \alpha_T, \beta, V_F, V_L, V_T$ , and  $r$  described in Table 2.1. The PCNN image signature was determined for each slice based on equation (2.6) summing to 50% (parameter described by 'areaCutOff' in Table 2.2) of the image space. This length N of each PCNN image signature vector was generally in the range of 40-50 iterations. The grayscale anatomy file was passed to the PCNN algorithm and the N binary output pulses for each slice

computed, which corresponds to  $A$  of equation (2.7) and held in variable 'binaryPCNNIterations'. This data was further processed by means of a binary morphological operation to break 'bridges', as described in section 2.2.3. The value of the 'bridge' radius  $p$  was set to 2 for this study. This setting allowed for small 'bridges' to be broken, early in the PCNN iteration. A higher value of the variable  $p$  would be useful when larger strands connect the brain tissue with surrounding tissue.

The neural network classifier in direct relation to the choice of the number of pulses had  $N$  input neurons, two hidden layers of 24 and 12 neurons and one output. For purposes of training, 7 rat volumes were used, each containing 12 slices. The activation function of the hidden layer was chosen to be a nonlinear hyperbolic tangent function while that of the output layer was linear. The 'newff' and 'train' functions available in Matlab 2007b's Neural Network toolbox V5.1 was used to train the classifier using the gradient descent with momentum backpropagation algorithm.

```

function [autoCroppedBrainVolume(nrow,ncol,nslice)] =
autoCrop[grayscaleAnatomy(nrow,ncol,nslice), areaCutOff, PCNNInputParametersVector]

for i = 1 : nslice

    j = 1; PCNNImageSignature(i,j) = 0;

    while (PCNNImageSignature(i,j))/(nrow * ncol) <= areaCutOff

        // PCNN returns binary array A on input of S (see equations (2.1) - (2.7))

        binaryPCNNIterations(:, :, i, j) = PCNN(grayscaleAnatomy(:, :, i), PCNNInputParametersVector), j)

        // binary morphological operator to break 'narrow bridges' with a radius less than p pixels.

        binaryPCNNIterations(:, :, i, j) = breakBridges(binaryPCNNIterations(:, :, i, j), p)

        // assuming largest area of corresponding iteration contain the desired brain mask

        binaryPCNNIterations(:, :, i, j) = largestArea(binaryPCNNIterations(:, :, i, j))

        // stores image signature in vector form

        PCNNImageSignature(i, j) = area(binaryPCNNIterations(:, :, i, j))

        // increment counter

        j = j+1;

    end

    // determines iteration

    choiceOfIteration = preTrainedNeuralNetworkClassifier(PCNNImageSignature(i, :))

    autoCroppedBrainVolume(:, :, i) = binaryPCNNIterations(:, :, i, choiceOfIteration)

end

```

**Table 2.2.** Pseudo code of rat brain cropping algorithm.

## 2.4 Discussion

### 2.4.1 Results

The PCNN based automated algorithm was tested on 42 volumes acquired on the three different rat brain acquisition parameter settings, described in Section 2.3. These volumes were different from the 7 data volumes used to train the ANN for automatic cropping. The compute time of the algorithm including original volume input (4.7 T,  $256 \times 256 \times 12$  anatomy volume) to cropped and mask volume outputs is about 5 minutes on a modern Pentium 4 class machine with 4GB RAM. Figure 2.8 provides a qualitative handle of the results obtained using the proposed PCNN based brain extraction algorithm compared to BET.

For purposes of numerical validation, we created manual masks for each of the volumes, employing MIVA (<http://ccni.wpi.edu/miva.html>) with the Swanson (Swanson, 1998), Paxinos and Watson (Paxinos and Watson, 1998) rat atlases for reference. The manually created masks served as the ‘gold’ standard. For a quantitative metric, we employed the Jaccard’s index (Jaccard, 1912). This index is a similarity measure in the range  $[0, 1]$ , where 1 describes an ideal match between the subject mask  $A_{Sub}$  generated by the proposed algorithm and the ground truth represented by the manually created mask  $M_G$  for that subject. The Jaccard similarity index is defined by:

$$Jaccard = \frac{|A_{Sub} \cap M_G|}{|A_{Sub} \cup M_G|}$$

We computed these indices using our automated PCNN algorithm for all volumes and summarized the results in Table 2.3. It has been established that popular automated brain extraction methods such as BET (Smith, 2002) have been inherently developed for cropping the human brain and offer lesser performance in cropping rat brain volumes (FSL). In the interest of experimentation we conducted tests on our rat brain volumes using BET V2.1. The average Jaccard index for these tests is also reported in Table 2.3. To obtain the highest BET score we scaled the rat brain image dimensions by a factor of 10 (Schwarz et al., 2007). We then manually specified the centre coordinates and initial radius of the rat brain for each individual animal. The fractional intensity threshold was iterated to 0.3 since the default setting of 0.5 yielded poor results.

A paired Student's t-test was conducted on the 4.7 T anatomy (256x256) dataset to test the null hypothesis that difference of means between the PCNN cropping method and BET V2.1 are a random sample from a normal distribution with mean 0 and unknown variance. The one tailed test on 30 volumes yielded a P value < 0.0001, effectively rejecting the null hypothesis at a 99.999 % confidence level in support of the alternate hypothesis that the mean Jaccard index of the PCNN method is higher than that of BET V2.1 for the 4.7 T anatomy (256x256) dataset. The corresponding t value equaled -14.06 and degrees of freedom were 29.

Dataset, Method	Mean	Std. dev.	Median	Min	Max
4.7 T Dataset (256×256), PCNN	0.93	0.02	0.94	0.89	0.94
4.7 T Dataset (256×256), BET	0.84	0.04	0.85	0.70	0.85
4.7 T Dataset (128×128) 2D rebinning, PCNN	0.92	0.02	0.92	0.88	0.94
4.7 T fMRI Dataset (64×64), PCNN	0.91	0.03	0.91	0.87	0.95
9.4 T Dataset (256×256), PCNN	0.95	0.01	0.95	0.94	0.96
9.4 T Dataset (256×256), BET	0.78	0.05	0.78	0.71	0.84
9.4 T Dataset (128×128) 2D rebinning, PCNN	0.93	0.02	0.94	0.91	0.95

**Table 2.3.** Lists the performance metrics of the automatic PCNN, BET V2.1 on the three different datasets described in the paper.

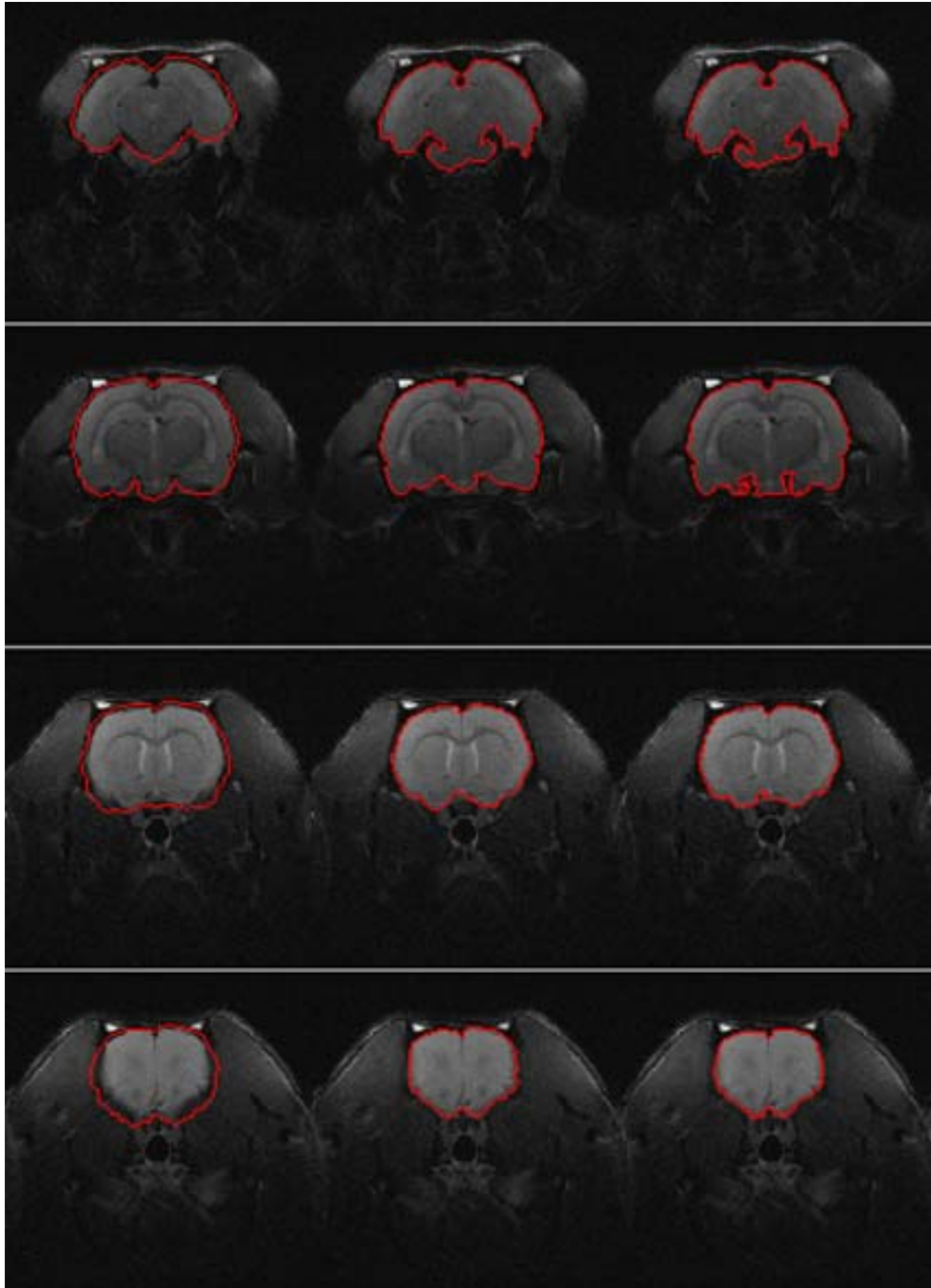


**Figure 2.8.** The 3 columns (L to R) represent the contours of the brain mask predicted by BET (Jaccard index 0.84), Manual gold standard (Jaccard index 1.0) and the Automatic PCNN (Jaccard index 0.95) overlaid on the corresponding anatomy image.

These results support our proposed automated brain extraction algorithm for small animals such as rats, as the BET results are significantly lower than that presented using the PCNN strategy.

The PCNN as an algorithm has outstanding segmentation characteristics and is such independent of the image orientation and voxel dimension scaling. The PCNN readily segments the entire rat brain volume as delineated by Paxinos and Watson 1998, (+6 to -15mm AP in a coronal plane passing through Bregma). However, our current selection strategy identifies the largest area within the PCNN iteration mask. This poses a problem in extreme coronal slices ( $> +7\text{mm AP}$ ) where the eyes are larger and brighter as a result of T2 weighting, than the brain region. Surface coils can inherently lower sensitivities in regions distant from the coil diminishing overall image intensities. The PCNN operates only on 2D regions and one of the PCNN iterations would normally capture the brain anatomy and that iteration would be on the plateau (Figure 6) identified by the proposed selection strategy.

#### **2.4.2 Alternate PCNN iteration selection strategies**

The main contribution of this paper is the recasting of a complex 2D image segmentation task into a selection of an appropriate point a 1D time series curve. Several alternate strategies may be employed to automate or otherwise train the classifier. The accumulated response (Figure 2.6) can be modeled as a first order response system

$$firstOrderModel(pcnnIterationT) = heightFirstPlateau \left( 1 - \exp \left( \frac{-pcnnIterationT}{\tau_{pcnnIterationT}} \right) \right)$$

with the selected iteration corresponding to a value of  $2\tau_{pcnnIterationT}$ . Creating a trained ANN or augmenting an existing one can be done using the manual override option (Figure 2.5). To illustrate, if a blank trained ANN is used, the system predicts the N/2 iteration and displays a 3x3 grid centered about the predicted iteration. The iteration contours are superimposed on the grayscale image. If the identified iteration is acceptable (N/2 in this example), one accepts the default and the next slice is analyzed. If an alternate iteration is desired, the user identifies its number and the next slice is analyzed. The process is the same for any decision pathway selected (blank ANN, partially trained ANN, trained ANN, or First Order Response). If the user specifies a manual override option, the PCNN output will display the forecasted iteration for each slice allowing the user to override its selection. Once the volume set is analyzed the user has the option to merge the dataset responses into the trained ANN matrix.

## 2.5 Conclusion

A novel, brain extraction algorithm was developed and tested for automatic cropping of rat brain volumes. This strategy harnessed the inherent segmentation characteristics of the PCNN to produce binary images. These image masks were mapped onto a timeline curve rendering the task into an appropriate iteration

selection problem. The surrogate 'time' signature was passed to a previously trained ANN for final iteration selection. The algorithm was tested on rat brain volumes from 3 different acquisition configurations and quantitatively compared against corresponding manually created masks which served as the reference. Our results conclusively demonstrate that PCNN based brain extraction represents a unique, viable fork in the lineage of the various brain extraction strategies.

## **2.6 Supplementary Material**

The PCNN code and data (4.7T 256×256×12 anatomy volumes, 'Gold' standard masks) described in this chapter are available as a supplementary download (NeuroImage/Elsevier web products server) on a 'Non profit, academic/research use only' type of license. The included code is suitable for a Matlab 2007b environment with Image Processing Toolbox V2.5 and Neural Network Toolbox 5.1.

## Chapter 3

### Multiple region segmentation using a PCNN

#### 3.1 Introduction:

Automatic brain tissue segmentation into GM (Grey Matter), WM (White Matter) and CSF (Cerebro-Spinal Fluid) classes is a basic requirement for conducting quantitative statistical tests on large sets of subjects (Cocosco, et al. 2003), (Zijdenbos, et al. 2002) and GM atrophy detection and monitoring in patients with multiple sclerosis (MS) (Nakamura and Fisher 2009). Published brain tissue classification approaches may be broadly classified based on the principal image segmentation (Pham, et al. 2000) strategy employed: Thresholding (Schnack, et al. 2001), Classifier based (Ashburner and Friston 2005; Hasanzadeh and Kasaei 2008), a priori Atlas-Guided, Clustering, Deformable models, Markov Random Field Models (Rivera, et al. 2007) and Artificial Neural Networks (Reddick, et al. 1997). Most recent published methods are hybrids, employing combinations of several image segmentation methods (Cocosco, et al. 2003; Nakamura and Fisher 2009) to improve voxel classification accuracy.

In this paper we introduce the Pulse Coupled Neural Network (PCNN) as a viable multiple material segmentation algorithm. The PCNN is based on neurophysiological studies of the primary visual cortex of a cat by Eckhorn et al.(1990). They developed a neural network model that captured the observed global linking of cell assemblies

as a result of feature similarity in sensory systems. The specific algorithm used in this article is the Eckhorn (Eckhorn, et al. 1990) model implemented by Johnson and Padgett (1999) and Waldemark et al. (2000). In this formulation, the PCNN operates on 2D grayscale data. In Figure 1b through Figure 1f, we graphically illustrate the segmentation characteristics of the PCNN operating in ‘*accumulate*’ mode (discussed subsequently), on a cropped T1 weighted brain data (from volume 1\_24, IBSR), Figure 3.1a (IBSR). In this illustration, the accumulated iterations are capped at unity. By observation, the problem is one of identifying which iteration yields the best segmentation. Note that in Figure 3.1f, the PCNN iteration number 110 bleeds into the zero intensity region beyond the cropped brain anatomy. Subsequent PCNN iterations would fill up the entire 2D space.

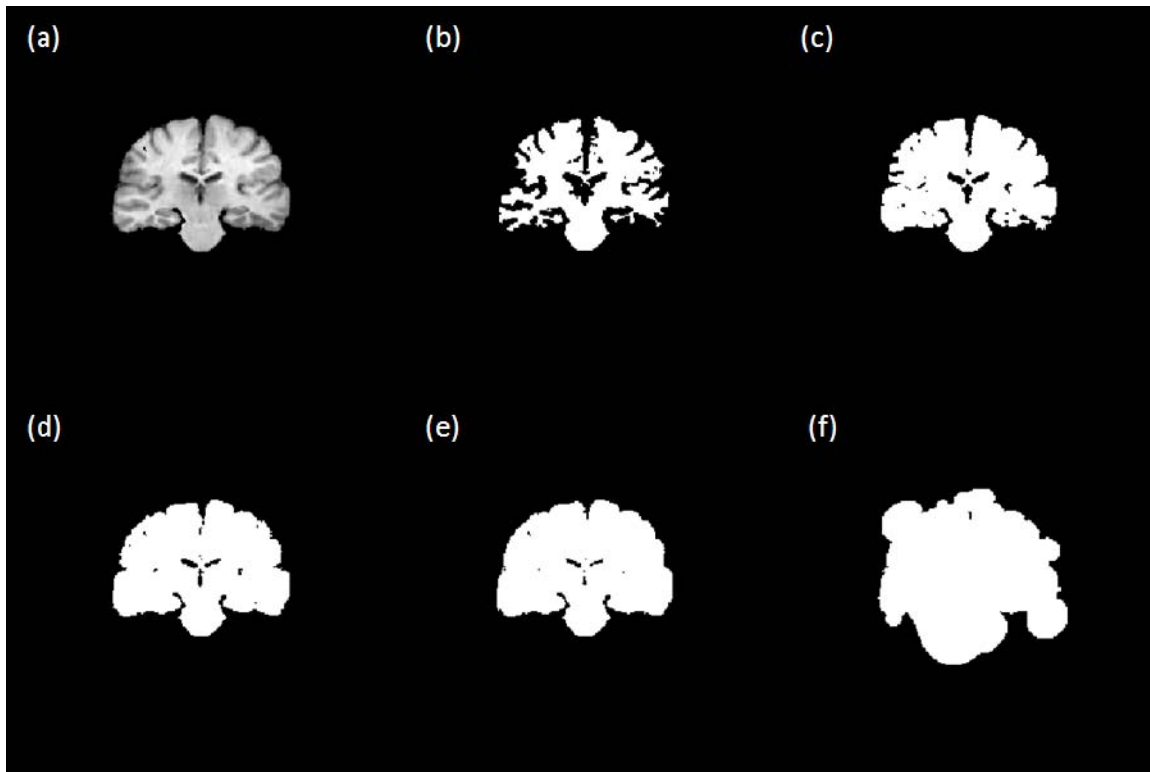


**Figure 3.1.** Subfigure (a) is a sample cropped grayscale slice from the IBSR volume 1\_24. Subfigures (b)-(f) illustrate the raw, accumulated *binary* PCNN iterations 5,10,15,20 and 110 respectively.

The PCNN (Murugavel and Sullivan Jr. 2009a) has successfully been used to automatically crop T2 weighted rat brain volumes. Figure 3.2 illustrates sample results obtained. The reported PCNN algorithm was engaged in ‘accumulate’ mode on individual grayscale slices and thresholded at unity. A morphological operator was applied to break ‘bridges’ that thinly connected large adjacent regions. The algorithm selected the largest contiguous area from each PCNN iteration. The binary area occupied at each PCNN iteration was used as a time series signature on the lines of Muresan (2003) to train an ANN (Artificial Neural Network) to effect successful cropping.

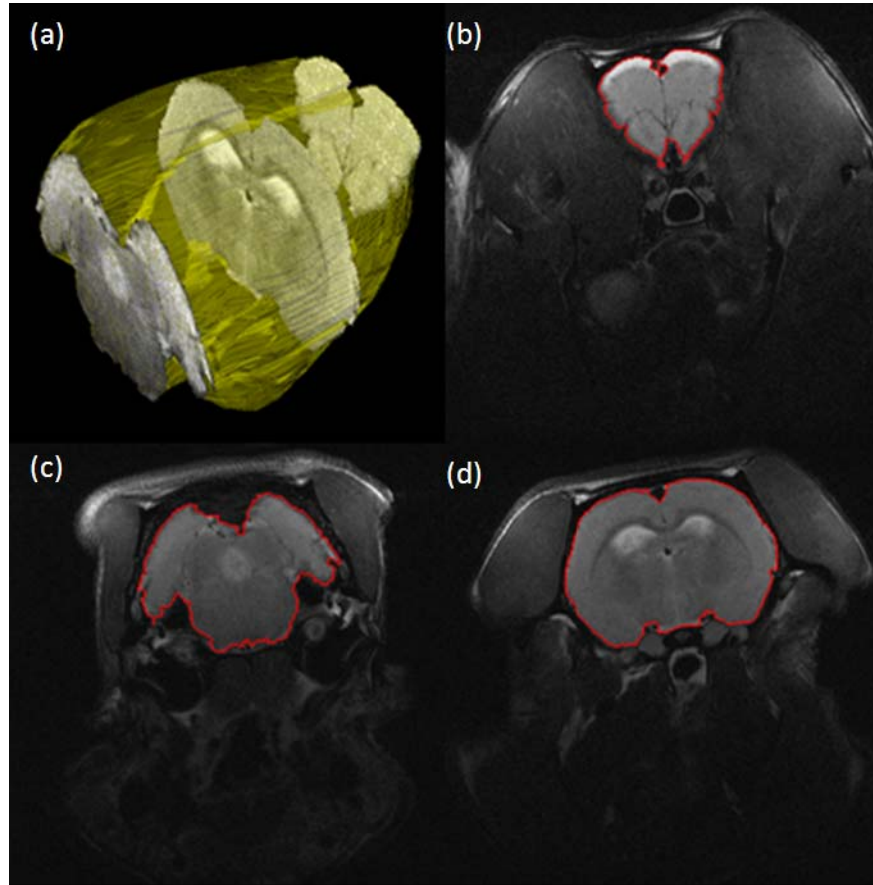


**Figure 3.2.** Subfigure (a) illustrates a 3D surface mesh (Ziji Wu 2003) of the rat brain overlaid with 3 cropped grayscale slices. Subfigures (b) – (d) illustrate the brain masks obtained using the automatic PCNN algorithm (Murugavel and Sullivan Jr. 2009a).

The work herein is focused on segmentation of brain tissue rather than brain cropping. Brain extraction or cropping is essentially a subset of general image segmentation strategies (Murugavel and Sullivan Jr. 2009a) wherein one material (the brain) is segmented from surrounding tissue.

## 3.2. Materials and Methods

### 3.2.1 The Eckhorn Pulse Coupled Neural Network:

The PCNN operates on 2D grayscale intensity images described by variable  $S_{ij}$  with  $i, j$  describing the location of each grayscale pixel and the corresponding PCNN 'neuron'. Each PCNN neuron is directly coupled to a set of neighboring neurons encompassed by a predefined radius  $r$ , known as the 'linking field' (Waldemark, et al. 2000). The functionality is effected by means of a Feeding and Linking compartment, described by arrays  $F_{ij}$  and  $L_{ij}$ , each of dimension equaling the 2D input grayscale image, linked by two synaptic weighting matrices  $M$  and  $W$ . The synaptic weighting matrix is square with a dimension of  $(2r + 1)$  and is a normalized Gaussian about the center of the square matrix.

$$F_{ij}[n] = e^{-\alpha_F} F_{ij}[n-1] + S_{ij} + V_F (M * Y[n-1])_{ij} \quad (3.1)$$

$$L_{ij}[n] = e^{-\alpha_L} L_{ij}[n-1] + V_L (W * Y[n-1])_{ij} \quad (3.2)$$

$$U_{ij}[n] = F_{ij}[n] (1 + \beta L_{ij}[n]) \quad (3.3)$$

$$T_{ij}[n] = e^{-\alpha_T} T_{ij}[n-1] + V_T Y_{ij}[n]$$

(3.4)

$$Y_{ij}[n] = 1 \text{ if } U_{ij}[n] > T_{ij}[n] \quad (3.5)$$

$$Y_{ij}[n] = 0 \text{ if } U_{ij}[n] \leq T_{ij}[n] \quad (3.6)$$

The PCNN is implemented by iterating through equations (3.1)-( 3.6) with  $n$  as the current iteration index and ranging from 1 to  $N$  (the total number of iterations). The matrices  $F_{ij}[0], L_{ij}[0], U_{ij}[0]$  and  $Y_{ij}[0]$  were initialized to a zero matrix, while  $T_{ij}[0]$  was initialized to a unit matrix. For each iteration, the internal activation  $U_{ij}$  is computed and compared against the threshold  $T_{ij}$ . Thus, the array  $Y_{ij}[n]$  is a binary image representing the PCNN mask at that particular iteration.

The PCNN coefficients used in this article were originally sourced from the work of Johnson and Padgett (1999) and Waldemark et al. (2000). The same constants were used for rat brain cropping (Murugavel and Sullivan Jr. 2009a).  $\alpha_F, \alpha_L, \alpha_T$  are iteration (surrogate time) constants that determine the internal state of the network effecting exponential decay and  $V_F, V_L, V_T$  are magnitude scaling terms for Feeding, Linking and Threshold components of the PCNN.  $*$  is the two dimensional convolution operator.  $\beta$  is a parameter affecting linking strength, Table 3.1.

Constant	PCNN coefficient	Context
$\beta$	0.2	Linking strength
$\tau_F$	0.3	Feeding decay
$\tau_L$	1	Linking decay
$\tau_T$	10	Threshold decay
$V_F$	0.01	Feeding coupling
$V_L$	0.2	Linking coupling
$V_T$	20	Magnitude scaling term for threshold
$r$	3	Radius of linking field

**Table 3.1:** The values of the PCNN coefficients used in this algorithm were sourced from Johnson and Padgett (1999) and Waldemark, et al. (2000). Further coefficients  $\alpha_{F,L,T} = \ln 2 / \tau_{F,L,T}$  as described by Waldemark, et al. (2000).

Our implementation of the PCNN operates in the ‘accumulate’ mode: that is, each iteration sums its contributions with the previous PCNN iterations.

$$A_{ij}[n] = \sum_{k=1}^n Y_{ij}[k] \quad (7)$$

### 3.2.2 Minimum Error Thresholding

The segmentation effected by the PCNN was characterized by the multiple threshold clustering method proposed by Kittler and Illingworth (1986). A recent review paper by Sezgin and Sankur (2004) surveyed and quantitatively compared the performance of 40 different thresholding methods categorized by the information space the methods exploit. The domains spanned histogram shape, measurement space clustering including fuzzy algorithms, entropy including cross entropy and fuzzy entropy methods, object attributes, spatial correlation and locally adaptive thresholding methods. Their study ranked the method of Kittler and Illingworth (1986) as the top performer among the 40 different methods surveyed. Within the MRI segmentation domain, the minimum error thresholding method has found application in initializing the FCM (Fuzzy C Means) clustering component of the unsupervised T1 weighted MRI brain segmentation algorithm proposed by Xue et al. (2003).

Consider a grayscale image  $s$ , with gray levels  $g$ , whose histogram  $h(g)$  has  $m$  modes representing a mixture of  $m$  normal densities. Kittler and Illingworth (1986) had shown the optimal separation thresholds  $X_i$  can be obtained at the minimum of the criterion,  $J$ , described by equation 8.

$$J(X_1, \dots, X_{m-1}) = 1 + 2 \times \sum_{i=1}^m \{P_i(X_i) [\log \sigma_i(X_i) - \log P_i(X_i)]\}, \quad (3.8)$$

where *a priori* probability  $P_i(X_i)$ , modal mean  $\mu_i(X_i)$ , and standard deviation  $\sigma_i(X_i)$  are described by equations (3.9) – (3.12).

$$P_i(X_i) = \sum_{g=X_{i-1}+1}^{X_i} h(g), \quad (3.9)$$

$$\mu_i(X_i) = \frac{1}{P_i(X_i)} \sum_{g=X_{i-1}+1}^{X_i} gh(g), \quad (3.10)$$

$$\sigma_i^2(X_i) = \frac{1}{P_i(X_i)} \sum_{g=X_{i-1}+1}^{X_i} [g - \mu_i(X_i)]^2 h(g) \quad (3.11)$$

and

$$\begin{aligned} X_m &= \text{totalNumberOfGreyLevels}, \\ X_0 &= -1. \end{aligned} \quad (3.12)$$

### 3.2.3 1D ‘Time signature’ representation of multi region segmentation

In this section we demonstrate the idea of the multi-threshold extension of Kittler and Illingworth’s (1986) method to generate a stopping criterion for the PCNN iteration.

If *a priori* information on the number of regions,  $nRegions$ , were available, it is possible

to compute the corresponding segment proportion ( $\gamma_{S_{n_i}}$ , with  $\sum_{i=1}^{nRegions} \gamma_{S_{n_i}} = 1$  and  $\gamma_{S_{n_i}} \geq 1$

), mean ( $\mu_{S_{n_i}}$ ) and standard deviation ( $\sigma_{S_{n_i}}$ ). Since the minimum error criterion (see

equation (3.8)) is based on the minimization of the Kullback Information distance

(Demirkaya et al. 2009; Haralik and Shapiro 1992), we can construct a time series

representation of the multiple region segmentation on the lines of equation (3.8).

$$Js(n) = 1 + 2 \times \sum_{i=1}^{nRegions} \{ \gamma s_{n_i} [\log \sigma s_{n_i} - \log \gamma s_{n_i}] \} \quad (3.13)$$

The minimum of this function was found to yield the optimal segmentation among the various PCNN iterations with  $nRegions$ . We illustrate this procedure on a simulated dataset provided by IBSR. Figure 3.3(a) shows a 3 region shape phantom with a Signal to Noise Ratio (SNR) of 15. We introduced a cropping on the original dataset to better represent the cropped brain anatomy, comprising of 3 regions CSF, GM and WM. Figure 3.3(b) illustrates the corresponding PCNN time series signature. The segmentation corresponding to the minimum value on the curve is selected and presented in Figure 3.3(c).

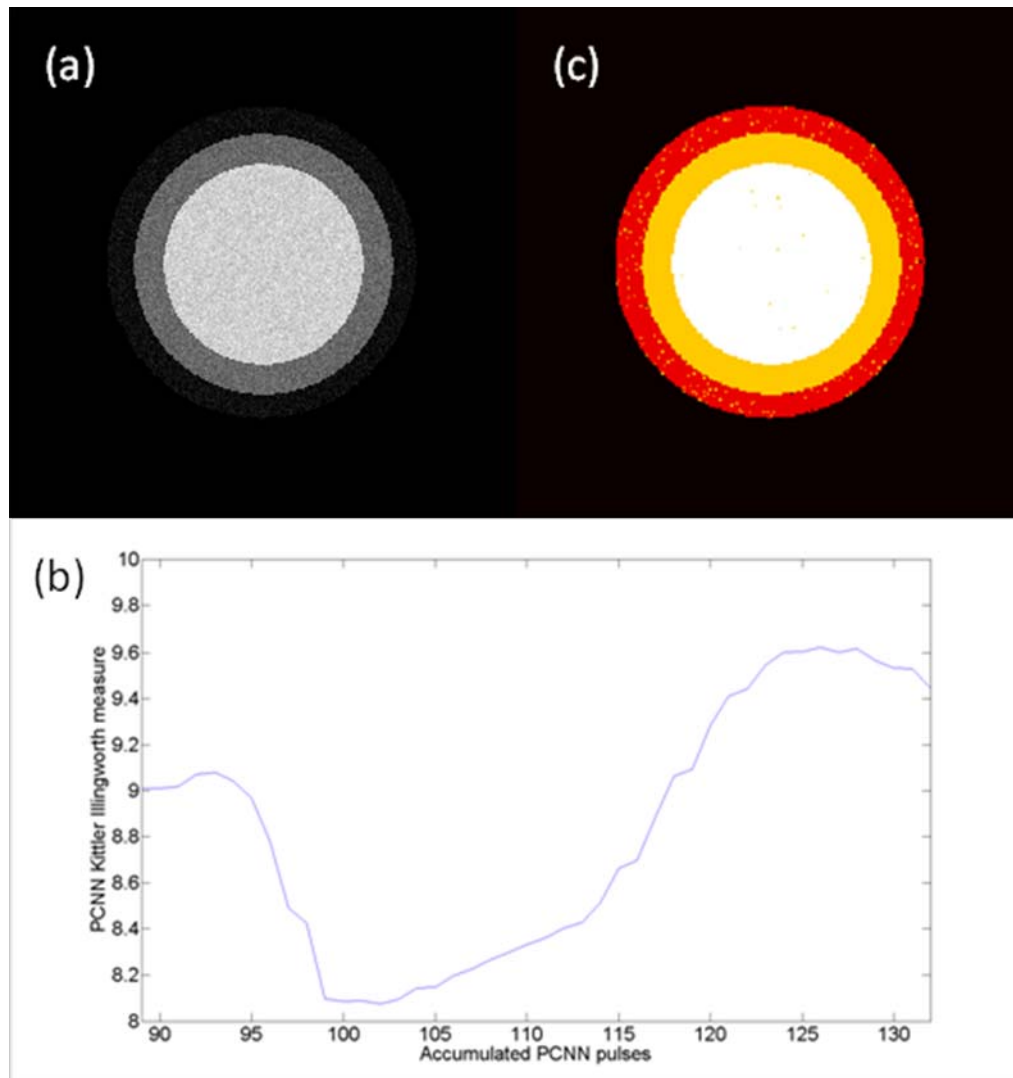


**Figure 3.3.** Illustrates the adaptation of the Kittler Illingworth (1986) method to segment multiple regions on a simulated dataset. Figure 3(a) shows a 3 region grayscale image (IBSR simulated data) corrupted with noise (SNR = 15). Figure 3.3(b) is a plot of the computed PCNN Kittler – Illingworth time measure for 3 regions against the corresponding accumulated PCNN iterations. Figure 3.3(c) shows the accumulated pulse 102, which corresponds to the minimum of the time series representation in Figure 3.3(b).

### 3.2.4 ANN based selection

Posing the 2D segmentation problem as a 1D time series signature enables the option of training an ANN to select the appropriate PCNN iteration. Multi Layer Perceptron (MLP) is a widely used supervised feedforward ANN model (Haykin 1998; Murugavel and Sullivan Jr. 2009a) that can be trained via standard backpropagation algorithms to map a vector of inputs to a suitable output. Figure 3.4 illustrates accumulated PCNN iterations  $A[n]$  (described by Equation (3.7)) of the grayscale brain slice illustrated in Figure 3.1(a). Each accumulated PCNN iteration yields a potential segmentation. Subfigure 3.4(a) is the third accumulated PCNN iteration and consists of only 1 region (WM). Subfigure 3.4(b) consists on only one region, but is included to highlight the opportunity it accords to segment CSF, which is highlighted within the surrounding white colored region (combined WM and GM). Subfigures 3.4(c) and 3.4(d) encompass two regions WM (colored white) and GM (yellow). Subfigures 3.4(e) and 3.4(f), with included colorbars, are segmentations containing 4 and 5 regions respectively. Note that the brighter intensities correspond to WM; darker shades (orange, red) correspond to CSF while the mid intensities (yellow) correspond to GM.

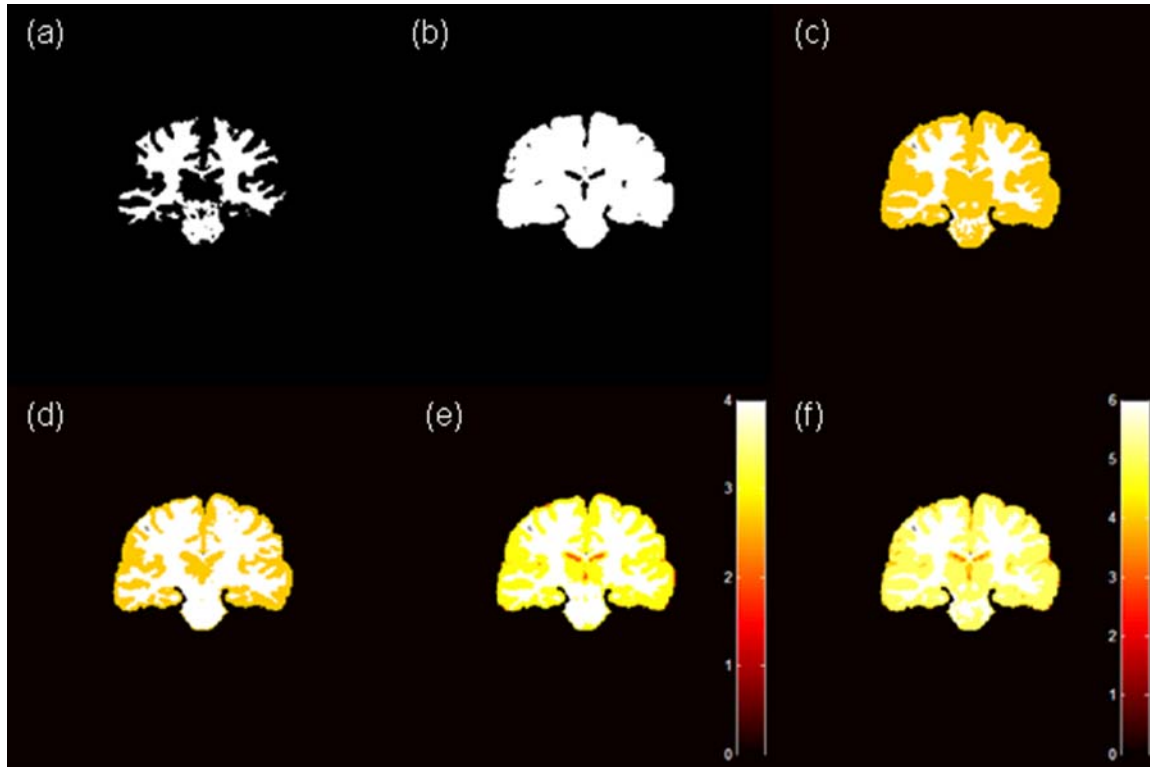


**Figure 3.4.** Subfigures (a)-(f) illustrate the raw, accumulated PCNN iterations 3, 13, 50, 54, 148 and 242 of the grayscale slice illustrated in Figure 3.1(a).

Figure 3.5 shows a characteristic 1D PCNN time signature based on the Kittler-Illingworth formulation (Equation 3.13, with number of regions set to two, GM and WM segmentation) for the grayscale slice described in Figure 3.1(a). The signature will be similar for a particular segmentation problem, for example GM, WM segmentation. In this work we generate a training set based on a single brain volume from the ISBR database (IBSR) by generating the PCNN image signatures for each grayscale slice  $s$  and automatically selecting the best GM-WM segmentation from the corresponding manual mask by maximizing the Jaccard Index (explained subsequently). Alternately, the best GM-WM segmentation may be

selected manually from among the various accumulated PCNN iterations as an interactive tool which can be used for training the MLP. This latter option is useful in situations where prior reference masks do not exist.

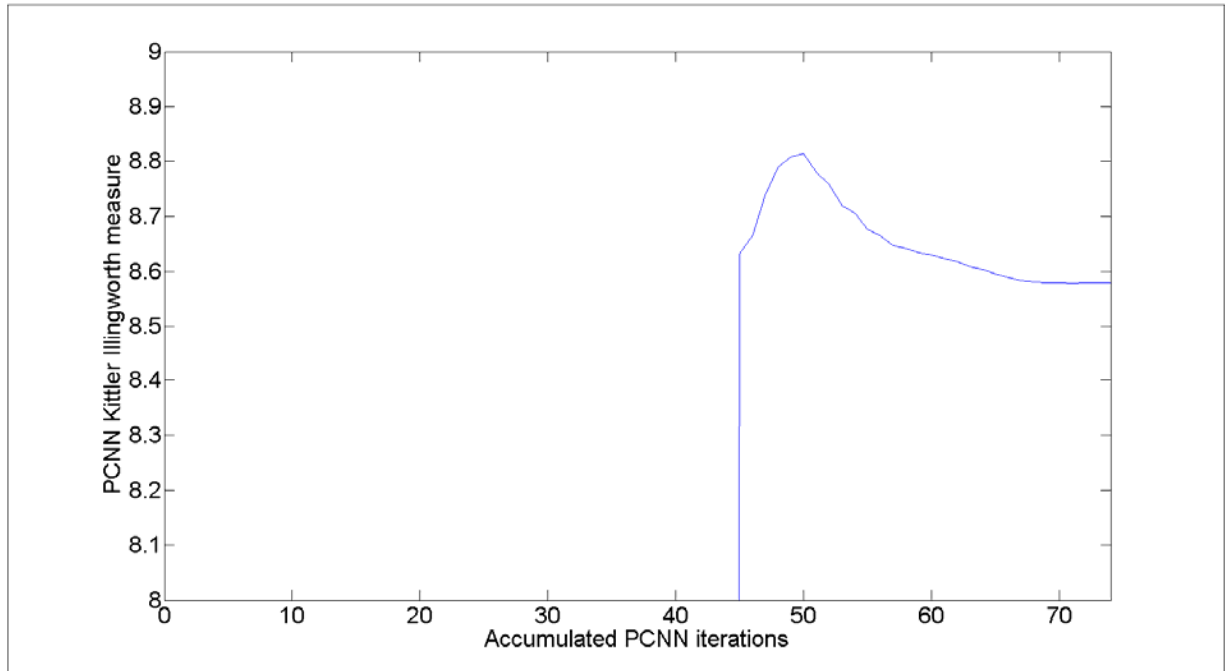


**Figure 3.5.** Plot of the computed PCNN Kittler – Illingworth time measure for 2 regions against the corresponding accumulated PCNN iterations.

The neural architecture of the MLP used in this article consists of one input layer, two hidden layers and a single output neuron. The input layer neurons directly map to the Kittler-Illingworth PCNN signature which is a vector of dimension  $N$ . The vector is normalized using the min-max method as described by Umbaugh, S.E. (2005) for efficient supervised training using the back propagation algorithm. The two hidden layers consisted of about  $0.5 N$  and  $0.25 N$  neurons, respectively. The single output neuron identifies the PCNN iteration corresponding to the best GM-WM segmentation.

### 3.2.5 Gaussian Mixture Model (GMM) based selection

GMM based methods have been widely adopted to address the GM-WM-CSF segmentation problem (Ashburner and Friston 2005). A distribution describing a grayscale image  $s$ , consisting of only those pixels within the cropped brain can be modeled by a mixture of  $k$  Gaussians (Ashburner and Friston 2005). This univariate mixture with pixel intensities  $x$ , can be represented as the following weighted summation of  $k$  class conditional probability distribution functions (Demirkaya, et al. 2009).

$$f(x) = \sum_{i=1}^k \gamma_i N(x | \mu_i, \sigma_i^2) \quad (3.14)$$

$$N(x | \mu_i, \sigma_i^2) = \frac{1}{(2\pi\sigma_i^2)^{\frac{1}{2}}} \exp\left(-\frac{(x - \mu_i)^2}{2\sigma_i^2}\right) \quad (3.15)$$

where  $\mu_i$ ,  $\sigma_i$ ,  $\gamma_i$  represent the mean, standard deviation and mixing proportion of class  $i$ . with  $\sum_{i=1}^k \gamma_i = 1$  and  $\gamma_i \geq 1$ .

The standard Expectation Maximization (EM) (Dempster, et al. 1977; Bishop 1995) algorithm can be used to as an estimator to generate a feature vector consisting of means, standard deviations and mixing proportions of the  $k$  Gaussians of each grayscale image,  $\hat{e} = [\mu_1 \dots \mu_k \ \sigma_1 \dots \sigma_k \ \gamma_1 \dots \gamma_k]$ . As described in Section 3.2.3, accumulated PCNN iterations  $A[n]$  may be computed for each grayscale image  $S$ . With access to a *priori* information on the number of regions (equal to  $k$ ), we can generate a feature vector for each PCNN

iteration,  $e_n = [\mu_{S_{n1}} \dots \mu_{S_{nk}} \sigma_{S_{n1}} \dots \sigma_{S_{nk}} \gamma_{S_{n1}} \dots \gamma_{S_{nk}}]$ , similar to the estimate  $\hat{e}$  from the GMM-EM formulation described in this section. In this implementation, the subscript  $n$  represents only those accumulated PCNN iterations with a total of  $k$  regions. The appropriate choice of the PCNN segmentation is simply that iteration  $n$ , which minimized the Euclidean norm  $\|\hat{e} - e_n\|$ . This strategy is unsupervised and requires no prior classifier training.

### 3.3. Experiment details

#### 3.3.1 Data

The 20 normal T1 weighted MR brain data sets and their manual segmentations were provided by the Center for Morphometric Analysis at Massachusetts General Hospital and are available at <http://www.cma.mgh.harvard.edu/ibsr/>.

#### 3.3.2 Parameters employed in the ANN based selection method

The algorithms described in the ANN based selection method is presented as pseudo code in Table 3.2. The algorithm was implemented in Matlab 2008a (Mathworks, MA, U.S.A.). The 19 input grayscale brain volumes from IBSR were treated as the subject data and individually addressed by the 'croppedGrayscaleAnatomy' variable in Table 3.2. The PCNN algorithm was implemented and the 'PCNNInputParametersVector' of Table 3.2 contained

numerical values of the various PCNN parameters,  $\alpha_F, \alpha_L, \alpha_T, \beta, V_F, V_L, V_T$ , and  $r$  described in Table 3.1. In this implementation, the number of regions, 'nRegions', was set to two (considered only GM and WM). CSF was ignored as it did not occur in all the slices and the overall proportion of CSF is negligible in comparison to GM and WM. Several researchers working with this dataset have either not reported CSF (Shan Shen, et al. 2005; Solomon, et al. 2006) or have pooled CSF and GM (Rivera, et al. 2007) voxels. The PCNN time series representation, 'kittlerIllingworthPCNNTimeSeries' was determined for each slice based on equation (3.13). The length of the time series vector was generally in the range of 80-90 iterations. This vector was normalized to length  $N = 84$  to match the pre-trained ANN classifier. The neural network classifier in direct relation to the choice of the number of pulses had  $N$  input neurons, two hidden layers of 40 and 12 neurons and one output. For purposes of training, a single human brain volume with the identifier '1\_24' consisting of 55 slices was used. The activation function of the hidden layer was chosen to be a nonlinear hyperbolic tangent function while that of the output layer was linear. The 'newff' and 'train' functions available in Matlab 2008a's Neural Network toolbox V6.0 were used to train the classifier using the gradient descent with momentum backpropagation algorithm.

### **3.3.3 Parameters employed in the GMM – EM based selection method**

The algorithms described in the GMM – EM based selection method is presented as pseudo code in Table 3.3. The algorithm was implemented in Matlab 2008a

(Mathworks, MA, U.S.A.). The 20 input grayscale brain volumes from IBSR were treated as the subject data and individually addressed by the 'croppedGrayscaleAnatomy' variable in Table 3.3. The PCNN algorithm was implemented and the 'PCNNInputParametersVector' of Table 3.3 contained numerical values of the various PCNN parameters,  $\alpha_F, \alpha_L, \alpha_T, \beta, V_F, V_L, V_T$ , and  $r$  described in Table 3.1. In this implementation, the number of regions, 'nRegions', was set to three (GM, WM and CSF were considered). The grayscale intensities of each individual 2D slice  $S$  were modeled as a mixture of three Gaussians and the basic EM algorithm described by the function 'gmm\_bayes\_em' operating with default parameters, available as part of the GMMBayes Toolbox Version 1.0 (open source GNU license, <http://www.it.lut.fi/project/gmmbayes>) was used to generate the estimated feature vector  $\hat{e} = [\mu_1 \dots \mu_k \sigma_1 \dots \sigma_k \gamma_1 \dots \gamma_k]$ . The Euclidean distance between the estimated feature vector described by the variable 'estimatedFeatureVector' and each of the individual feature vectors, described by variable 'featureVec' was computed, 'euclideanDistance'. The three region segmentation for each grayscale slice  $S$  is the accumulated PCNN iteration that corresponds to the minimum of the vector, 'euclideanDistance'.

```

function [segmentedBrainVolume(nrow,ncol,nslice)] =
autoSegPCNNTimeSeries[croppedGrayscaleAnatomy(nrow,ncol,nslice), PCNNInputParametersVector,
nRegions]
for i = 1 : nslice

    // PCNN returns accumulated array A on input of S (see equations (3.1) - (3.7)). Cropped brain mask
    // applied on each iteration. Function returns only accumulated PCNN iterations with a total of nRegions.
    accumulatedPCNNIterations = pcnnAccumulateMode(croppedGrayscaleAnatomy(: , : , i),
PCNNInputParametersVector, nRegions)

    // Determine number of PCNN pulses in the accumulatedPCNNIterations volume
    [nrow, ncol, noPulses] = size(accumulatedPCNNIterations)

    // Initialize Kittler-Illingworth based time series vector
    kittlerIllingworthPCNNTimeSeries(1 : noPulses) = 0

    // Begin loop to compute the time series vector
    for j = 1 : noPulses
        if noRegions(accumulatedPCNNIterations(: , : , i) ) == nRegions
            kittlerIllingworthPCNNTimeSeries(j) =
                computeKittlerIllingworthMeasure(accumulatedPCNNIterations(: , : , i)
        end
    end

    // Normalize the time series vector to Length N and range 0 to 1 (see Section 3.2.4)
    kittlerIllingworthPCNNTimeSeries = minMaxAndLengthNorm(kittlerIllingworthPCNNTimeSeries)

    // Begin ANN based prediction
    segmentedBrain(nrow, ncol, i) = preTrainedNeuralNetworkClassifier(kittlerIllingworthPCNNTimeSeries)
end

```

**Table 3.2.** Pseudo code of PCNN – ANN based selection method

```

function [segmentedBrainVolume(nrow,ncol,nslice)] =
autoSegPCNNGaussian[croppedGrayscaleAnatomy(nrow,ncol,nslice), PCNNInputParametersVector, nRegions]
for i = 1 : nslice

    // PCNN returns accumulated array A on input of S (see equations (3.1) - (3.7)). Cropped brain mask
    // applied on each iteration. Function returns only accumulated PCNN iterations with a total of nRegions.
    S = croppedGrayscaleAnatomy(: , : , i)

    accumulatedPCNNIterations = pcnnAccumulateMode(S, PCNNInputParametersVector, nRegions)

    // Determine number of PCNN pulses in the accumulatedPCNNIterations volume
    [nrow, ncol, noPulses] = size(accumulatedPCNNIterations)

    // Estimate the means, standard deviations and mixing proportion of the nRegions (GM, WM and CSF) in
    // S [eMu1 .. eMunRegions eSD1 .. eSDnRegions eMp1 .. eMpnRegions] (see section 3.2.5)
    estimatedFeatureVector = gmmEM(S, nRegions)

    // Begin loop to compute feature vector (identical to the estimate ) for individual PCNN iterations, distance
    // measure
    for j = 1 : noPulses
        if noRegions(accumulatedPCNNIterations(: , : , i) ) == nRegions
            // compute feature vector [Muj,1 .. Muj,nRegions SDj,1 .. SDj,nRegions Mpj,1 ..
            // Mpj,nRegions]
            featureVec(j) =
                computeMeansStdDevProportions(accumulatedPCNNIterations, S)
            // Euclidean distance between estimate and computed feature vector of each
            // iteration
            euclideanDistance(j) = euclideanNorm(estimatedFeatureVec - featureVec(j))
        end
    end

    // Begin GMM – EM based selection. Select PCNN iteration corresponding to min of euclidean distance
    segmentedBrain(nrow, ncol, i) = minSelect(euclideanDistance, accumulatedPCNNIterations)
end

```

**Table 3.3.** Pseudo code of PCNN – GMM EM based selection method

## **3.4. Results and Discussion**

### **3.4.1 Results**

The PCNN based segmentation algorithms described in Sections 3.3.2 (PCNN time series – ANN) and 3.3.3 (PCNN – GMM – EM selection) were tested on the 20 volumes obtained from IBSR. A modern Pentium 4 class machine with 4 GB RAM was employed for testing each algorithm. The compute time of the PCNN time series – ANN selection algorithm including original volume input to segmented outputs is about 2 minutes. The PCNN – GMM – EM selection algorithm averaged about 4 minutes for each brain volume. Qualitative results obtained by the proposed methods are described in Figure 3.6 and compared against the manual masks provided by IBSR.

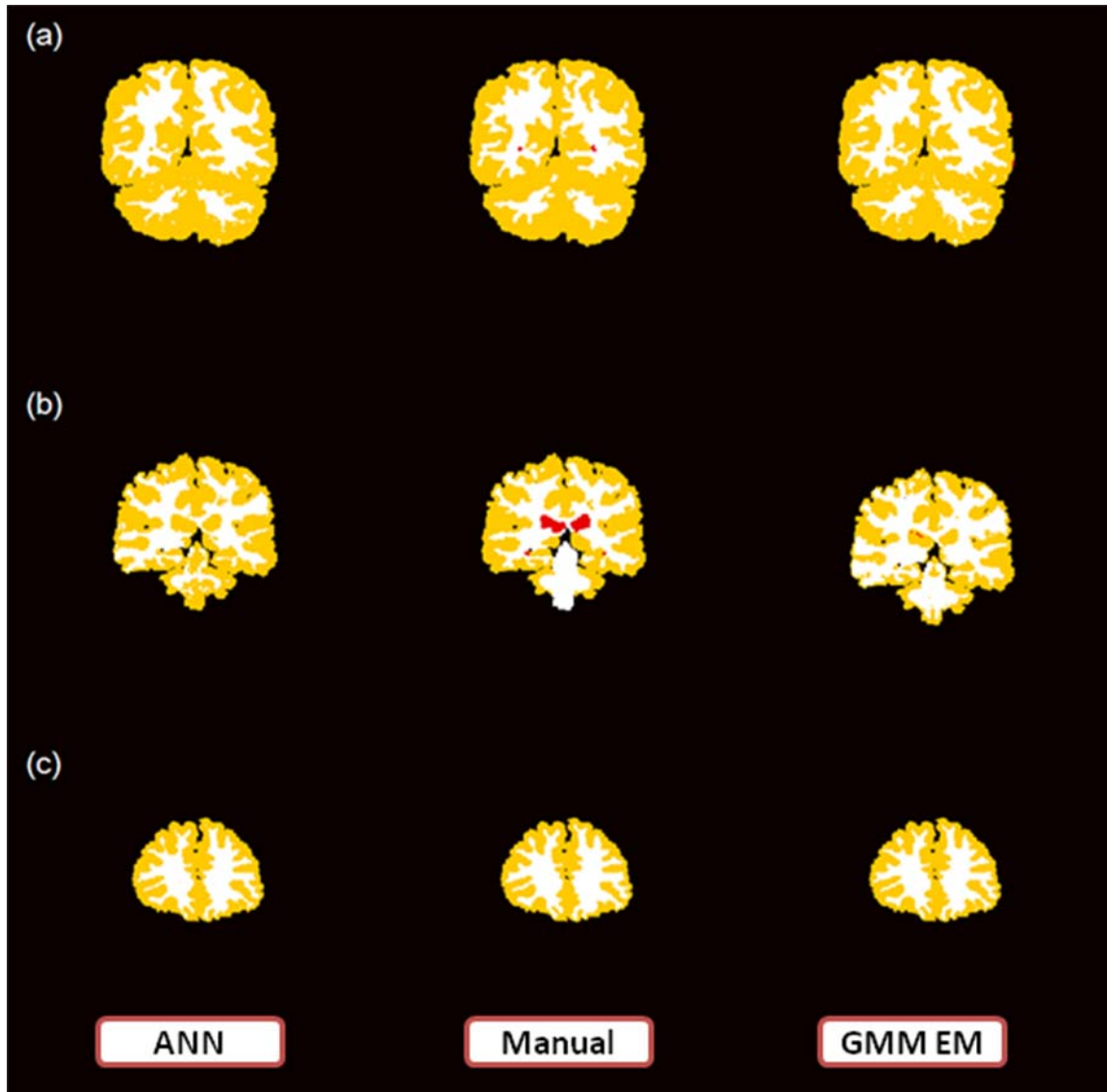


**Figure 3.6.** Qualitative comparison of the performance of the PCNN ANN and the PCNN – GMM EM algorithms is shown. Rows (a) through (c) span the brain spatially. The two extreme columns show segmentation results from the PCNN ANN and PCNN – GMM EM algorithms, respectively. The middle column shows the corresponding manual mask obtained from IBSR.

For purposes of numerical validation, the manual masks provided by IBSR were considered as the ‘gold standard’. As a quantitative comparison metric, we employed the Jaccard index (Jaccard 1912) for each class. This is identical to the Tanimoto coefficient (Duda and Hart 1973). Since Rajapakse and Kruggel (1998) this overlap metric has been employed by multiple researchers (IBSR publications) to report the performance of their respective methods on the IBSR data. For each region (GM, WM, CSF) this index is a similarity measure in the range [0, 1]. A numerical value of 1 for a particular region and subject, describes an ideal match between the corresponding mask  $A_{Sub,Region(i)}$  (with region index  $i$  ranging from 1 to number of regions) generated by the algorithm being evaluated and the ground truth represented by the ‘gold standard’ for that particular region,  $M_{G,Region(i)}$ . The Jaccard similarity index is defined by:

$$Jaccard_{Sub,Region(i)} = \frac{|A_{Sub,Region(i)} \cap M_{G,Region(i)}|}{|A_{Sub,Region(i)} \cup M_{G,Region(i)}|}$$

We computed these indices for each of the 20 volumes using the proposed PCNN time series – ANN and the PCNN – GMM – EM selection methods. The results obtained from our automated methods for each individual subject are summarized in Table 3.4. In Table 3.5 we have included a comprehensive comparison of the PCNN based methods against previously published methods on the IBSR data. These results demonstrate the viability of PCNN based segmentation strategies in addressing complex segmentation tasks.

Brain ID	PCNN - ANN selection		PCNN - EM selection		
	GM	WM	GM	WM	CSF
100_23	0.812	0.715	0.813	0.680	0.143
110_3	0.757	0.493	0.811	0.676	0.050
111_2	0.782	0.673	0.795	0.708	0.107
112_2	0.769	0.600	0.770	0.669	0.113
11_3	0.784	0.661	0.806	0.705	0.143
12_3	0.765	0.621	0.781	0.633	0.232
13_3	0.726	0.470	0.776	0.634	0.068
15_3	0.681	0.577	0.636	0.572	0.085
16_3	0.735	0.606	0.677	0.585	0.062
17_3	0.770	0.683	0.729	0.649	0.077
191_3	0.724	0.670	0.815	0.694	0.060
1_24	0.706	0.648	0.790	0.703	0.141
202_3	0.699	0.650	0.810	0.688	0.467
205_3	0.671	0.652	0.802	0.691	0.378
2_4	0.600	0.552	0.657	0.561	0.011
4_8	0.651	0.575	0.627	0.557	0.029
5_8	0.753	0.640	0.729	0.648	0.088
6_10	0.729	0.630	0.733	0.667	0.111
7_8	0.600	0.584	0.788	0.701	0.096
8_4	0.631	0.608	0.766	0.679	0.042

**Table 3.4** Jaccard indices obtained on each subject of the IBSR database for each class. Indices are presented for both the PCNN - ANN selection and the PCNN - GMM EM selection strategies.

Grey	White	CSF	Method	Reference
0.56	0.57	0.07	adaptive MAP	IBSR, Rajapakse and Kruggel (1998)
0.56	0.56	0.07	biased MAP	IBSR, Rajapakse and Kruggel (1998)
0.47	0.57	0.05	fuzzy c-means	IBSR, Rajapakse and Kruggel (1998)
0.55	0.55	0.07	Maximum A posteriori Probability (MAP)	IBSR, Rajapakse and Kruggel (1998)
0.53	0.55	0.06	Maximum-Likelihood	IBSR, Rajapakse and Kruggel (1998)
0.48	0.57	0.05	tree-structure k-means	IBSR, Rajapakse and Kruggel (1998)
0.53	0.64	n/a	fuzzy c-means with Neural Network Optimization	Shan Shen, et al. (2005)
0.58	0.69	n/a	Hidden Markov Model (16 volumes)	Solomon, et al. (2006)
0.59	0.63	0.21	Data-driven, Edge confidence, a priori information	Jimenez-Alaniz, et al. (2006)
<b>0.72</b>	<b>0.61</b>	<b>n/a</b>	<b>PCNN, time series, ANN selection (19 volumes)</b>	<b>Proposed (Section 3.2.4)</b>
0.66	0.68	n/a	Mamimizer of Posterior Marginals (MPM) MAP	Marroquin, et al. (2002)
0.77	0.67	n/a	Hidden Markov Model	Ibrahim, et al. (2006)
<b>0.76</b>	<b>0.66</b>	<b>0.13</b>	<b>PCNN, EM Maximization stopping</b>	<b>Proposed (Section 3.2.5)</b>
0.79	0.70	0.57	Fuzzy Membership connectedness	Maryam Hasanzadeh (2008)
0.82	0.74	n/a	Entropy controlled quadratic Markov measure field	Rivera, et al. (2007)
<b>0.88</b>	<b>0.83</b>	<b>n/a</b>	<b>Manual (4 brains averaged over 2 experts)</b>	IBSR

**Table 3.5.** Comprehensive comparison of published average Jaccard indices on the 20 T1 weighted volumes available at IBSR.

Two statistical tests were conducted to compare the performance of the PCNN-GMM-EM method against previously proposed methods, such as the Maximum Likelihood and tree-structure k-means (IBSR; Rajapakse and Kruggel (1998)). These two methods were chosen as their respective performance metrics (Jaccard index) were reported for individual volumes on IBSR. A paired Student's t-test was conducted to test the null hypothesis that difference of means between the PCNN-GMM-EM selection strategy and previously proposed methods (Maximum Likelihood, tree-structure k-means) are a random sample from a normal distribution with mean 0 and unknown variance. For GM, the one tailed test on 20 volumes yielded a P value  $< 0.0001$  for both methods (Maximum Likelihood, tree-structure k-means), effectively rejecting the null hypothesis at a 99.999 % confidence level in support of the alternate hypothesis that the mean Jaccard index of the PCNN- GMM-EM method is higher than that of Maximum Likelihood and tree structure k-means. The corresponding t values equaled -7.75 and -14.07 respectively. Similar tests on WM segmentation effectively rejected the null hypothesis at a reduced 95 % confidence level, with p values equaling 0.0101 (t value = -2.54) and 0.0244 (t value = -2.10) respectively for the Maximum Likelihood and tree structure k-means methods.

### **3.4.2 Discussion**

The main contribution of this paper is the demonstration and quantitative evaluation of the PCNN as a viable, multiple material segmentation strategy in automatically

segmenting T1 weighted MRI volumes. Previous pioneering work using the PCNN showed qualitative segmentation results (Keller and McKinnon 1999; Kuntimad and Ranganath 1999; Lindblad and Kinser 2005). However, they did not include quantitative evaluation on open databases. We further introduced a novel time series representation of a complex 2D multiple region segmentation task and demonstrated an ANN based method that can be rapidly adapted for various segmentation tasks. An unsupervised PCNN iteration selection strategy was introduced in the PCNN – GMM EM section. In Table 3.5, our highly successful automated results on 20 volumes compare well against manual results obtained on 4 brain volumes averaged over two experts. These results viewed against the backdrop of Figure 3.4 (see accumulated pulse numbers 148, 242 with number of regions  $> 3$ ) show qualitatively that accumulated PCNN iterations can approach a human eye's intensity delineation limits. Most recent segmentation methods require *a priori* information in the form of tissue probability maps (Jimenez-Alaniz, et al. 2006). While such an approach is clearly not suitable in situations where there is significant difference between the brain tissue atlas and the subject, it provides the option of improving subject voxel classification accuracy. For example, such prior information can be used to train two different classifiers (GM-WM, GM-WM and CSF) depending on the *a priori* prediction of the number of classes in a particular 2D grayscale slice. Hybrid methods (Ségonne, et al. 2004) involving pooling of results from multiple segmentation algorithms constitute another trend that could be adapted in augmenting PCNN based segmentation of brain tissue. The accumulated PCNN iteration that best matches the results from a different segmentation algorithm

will increase the overall probability of correct tissue classifications in the hybrid method.

### **3.5 Conclusions**

Two novel PCNN based algorithms (PCNN – ANN, PCNN – GMM EM) were developed and tested for automatic segmentation of human T1 weighted MRI brain volumes. The PCNN – ANN based selection method introduced the concept of a 1D time series representation of a 2D multiple material segmentation task. This signature was then used to train a ANN based classifier to automatically segment brain tissue into GM – WM classes. The PCNN – GMM EM method is completely unsupervised and was used to segment brain tissue into GM – WM – CSF. Both algorithms were tested on the 20 normal T1 weighted MRI brain volumes from Harvard's Internet Brain Segmentation Repository. Our quantitative results conclusively demonstrate that PCNN based multiple material segmentation strategies can approach a human eye's intensity delineation capability in grayscale image segmentation tasks.

### **3.6 Supplementary Material**

The PCNN code of the two algorithms described in this chapter will be made available as a supplementary download on a 'Non profit, academic/research use only' type of license. The included code is suitable for a Matlab 2008a environment with the corresponding Image Processing Toolbox and Neural Network Toolbox 6.0.

The 20 T1 weighted human brain volumes and their corresponding expert segmentations described in this article are available at <http://www.cma.mgh.harvard.edu/ibsr/>. The data will need to be converted into SDT/SPR (<http://www.cmrr.umn.edu/stimulate/stimUsersGuide/node57.html>) file format employed by programs such as MIVA (<http://ccni.wpi.edu/>) and Stimulate (<http://www.cmrr.umn.edu/stimulate/>). The GMMBayes Toolbox Version 1.0 (open source GNU license) used in the PCNN – GMM EM algorithm is available at, <http://www.it.lut.fi/project/gmmbayes>.

## Chapter 4

# Automatic cropping and segmentation of MRI breast volumes using Pulse Coupled Neural Networks

### 4.1 Introduction

Alternative breast imaging modalities such as MR Elastography (MRE), Electrical Impedance Spectroscopy (EIS), Microwave Imaging Spectroscopy (MIS) and Near Infrared Imaging (NIS) are being developed (Paulsen, et al. 2005). They are 'model-based' modalities (Paulsen, et al. 2005) requiring iterative, convergent, numerical techniques to map non-linear data to a target volume. MR image data is often used for comparison and validation purposes (Brooksby, et al. 2006). Frequently finite element models (FEM) for such applications are generated from MR images of the breast. Constructing a FEM requires cropping of the breast volume from the surrounding air and/or the receiver, driving transducer arrays of the alternate breast imaging modalities which are frequently in contact with the breast tissue during MR image acquisition. Predicting breast tissue deformation (Plewes, et al. 2000; Samani, et al. 2001; Lee, et al. 2009) via biomechanical modeling (FEM) of breast tissue is a necessary requirement for certain surgical and biopsy procedures which utilize images acquired under significant tissue deformation. Other applications of breast MR segmentation include tissue monitoring (Reichenbach, et al. 1999; Nie, et al. 2008), precursor to automated lesion classification (Ertaş, et al. 2008), volume registration (Gong and Brady 2008) and correlation studies between mammogram data and MR volumes (Wei, et al. 2004; Klifa, et al. 2004).

While MR based methods such as dynamic contrast – enhanced (DCE-MRI) have shown great potential as diagnostic tools in addressing breast cancer (Behrens, et al. 2007), our review of literature noted a lack of automated segmentation methods to specifically address breast MRI in comparison to for example, automatic MRI brain segmentation. Most breast MR segmentation is manual, semi-automated or involve simple thresholding methods. For example, Wei et al. (2004) describe a breast boundary detection with manual correction, followed by gray level thresholding and a morphological operator to exclude skin, Samani et al. (2001) use thresholding to segment fibroglandular and adipose tissue and Twellmann et al. (2005) uses the Otsu (Otsu 1979) thresholding method to crop breast tissue.

Other reported examples of MR breast tissue segmentation include, histogram fitting of Gaussians (Reichenbach, et al. 1998), Fuzzy C-Means (FCM) classification to exclude air and lung tissue with B-spline fitting to exclude chest wall muscle and dynamic searching to exclude skin (Nie, et al. 2008), Hidden Markov Random Measure Field model using expectation-maximization (EM) (Gong and Brady 2008), balloon snake segmentation to crop DCE-MRI volumes (Hill, et al. 2008) and Oriented Active Shape Models (Liu and Udupa 2009).

In this paper, we propose the PCNN (Pulse Coupled Neural Network) as a basic segmentation algorithm that can handle multiple segmentation tasks in breast MRI; such as automatic cropping of breast tissue followed by automatic or interactive

fibroglandular, adipose tissue segmentation. The PCNN used in this paper is based on the work of Eckhorn et al. (1990) who described synchronization in firing of otherwise distributed (spatially) biological neurons of small mammals such as cats in response to common stimulus features. This discovery has found multiple applications such as image segmentation (Keller and McKinnon 1999; Kuntimad and Ranganath 1999), image thinning (Gu, et al. 2004) and path optimization (Caulfield and Kinser 1999). A comprehensive description of the PCNN for image processing applications is described by Lindblad and Kinser (2005).

## **4.2 Materials and Methods**

### **4.2.1 Overview**

The proposed segmentation algorithm described in this paper consists of two independent algorithms each based on the PCNN. The first step is the cropping of the breast volume and is based entirely on the automatic rat brain cropping work of Murugavel and Sullivan (2009a). That algorithm is structured similarly to a PCNN based pattern recognition algorithm (Muresan 2003). Both the cropping and subsequent segmentation algorithms involved the generation of a 1D time signature from an image via a PCNN and a trained Multi Layer Perceptron (MLP) classifier to effect image segmentation and recognition, respectively. In this section we briefly describe the proposed two stage process. Figure 4.1 illustrates a sample 3D MR breast volume in coronal, sagittal and transverse orientations with transducer artifacts. Our breast cropping algorithm operates on 2D coronal grayscale data and

we track various operations on the 2D slice described by Figure 4.1(a). Each 2D slice is intensity normalized [0 1]. The PCNN is then applied in 'accumulate' (discussed subsequently) mode on each individual 2D slice, Figure 4.2. This operation is followed by a morphological operator which is designed to break narrow bridges that might connect transducer artifacts to the breast tissue, Figure 4.3. The largest, contiguous and enclosed area is selected by means of a contour operation at unity, Figure 4.4. The contour masks corresponding to the accumulated PCNN iterations are overlaid on the grayscale image, Figure 4.5. The accumulated response as a function of PCNN iteration has a characteristic signature as illustrated by Figure 4.6. The breast cropping task is reduced to simply identifying a PCNN iteration close to the beginning of the plateau region. Several techniques (Murugavel and Sullivan Jr. 2009a) can be used to identify the first plateau in Figure 4.6. A previously trained ANN can be used to identify the iteration that best represents the breast outline. An interactive mode also exists with the option to view the predicted selection and override that selection, Figure 4.5. This process is repeated for each slice resulting in a set of mask slices that can be used in a marching cube routine (Wu and Sullivan 2003) to create a full 3D geometry representation of the cropped breast, Figure 4.7.

The second step is based on the multiple material segmentation work described by Murugavel and Sullivan (2009b). The PCNN Kittler minimization and PCNN – GMM EM algorithms operate on cropped coronal tissue to segment fibroglandular and adipose tissue, Figure 4.8.

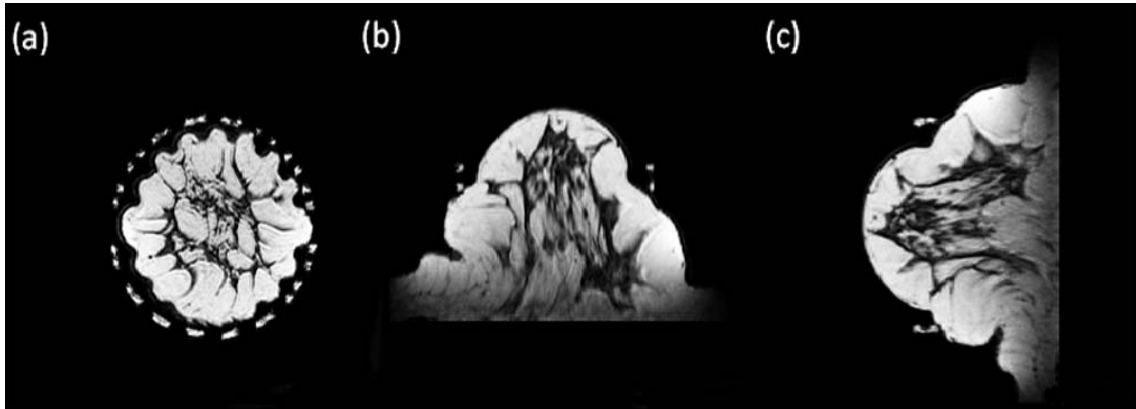


**Figure 4.1.** Subfigures (a) – (c) show coronal, sagittal and transverse sections of a breast volume. The serrated pattern observed on the periphery was caused by the transducer arrays positioned as required by the alternate breast imaging modalities such as NIS described in Section 4.1. The adipose tissue is generally of a higher intensity, while the darker irregular pattern constitutes fibroglandular tissue.

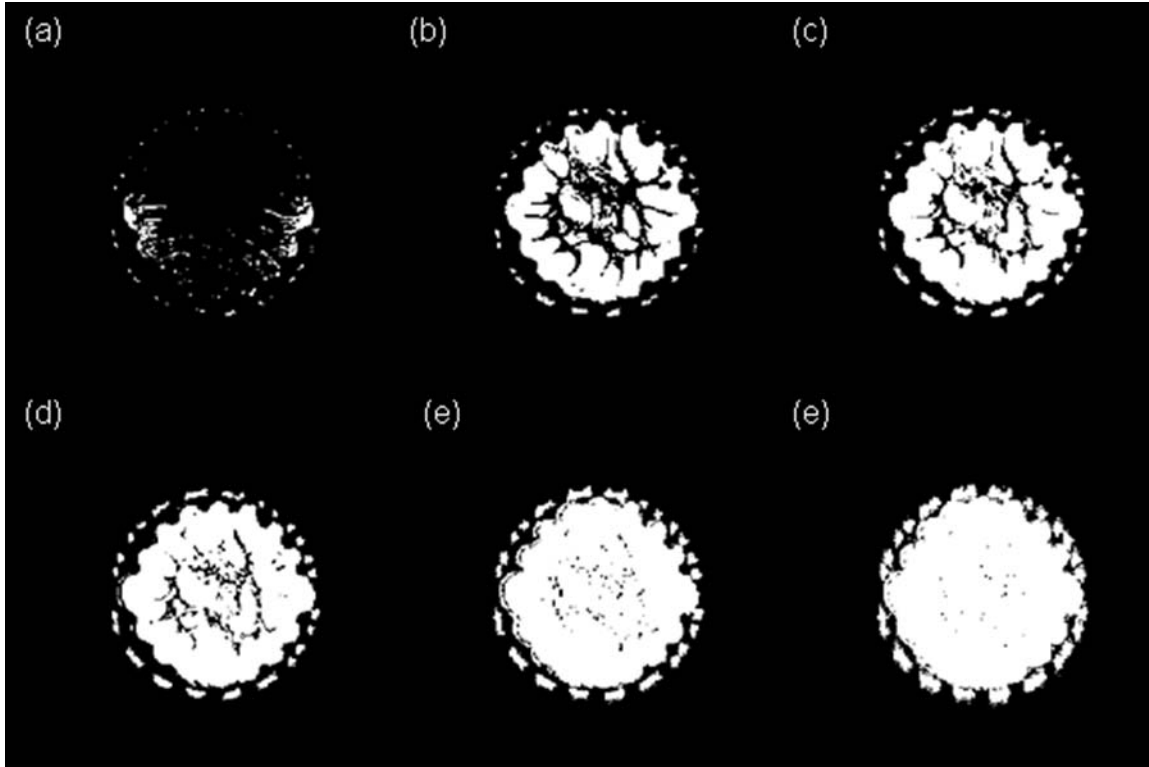


**Figure 4.2.** Subfigures (a) – (e) illustrate the raw, accumulated binary PCNN iteration numbers 5, 10, 15, 20, 30 and 40 respectively of the coronal grayscale slice of Figure 4.1(a).



**Figure 4.3.** Subfigures (L-R) show respectively, the accumulated PCNN iteration number 27 of the grayscale slice of Figure 4.1(a), detail of unbroken bridges highlighted in left figure before application of the morphological operator and detail after the application of the morphological operator.

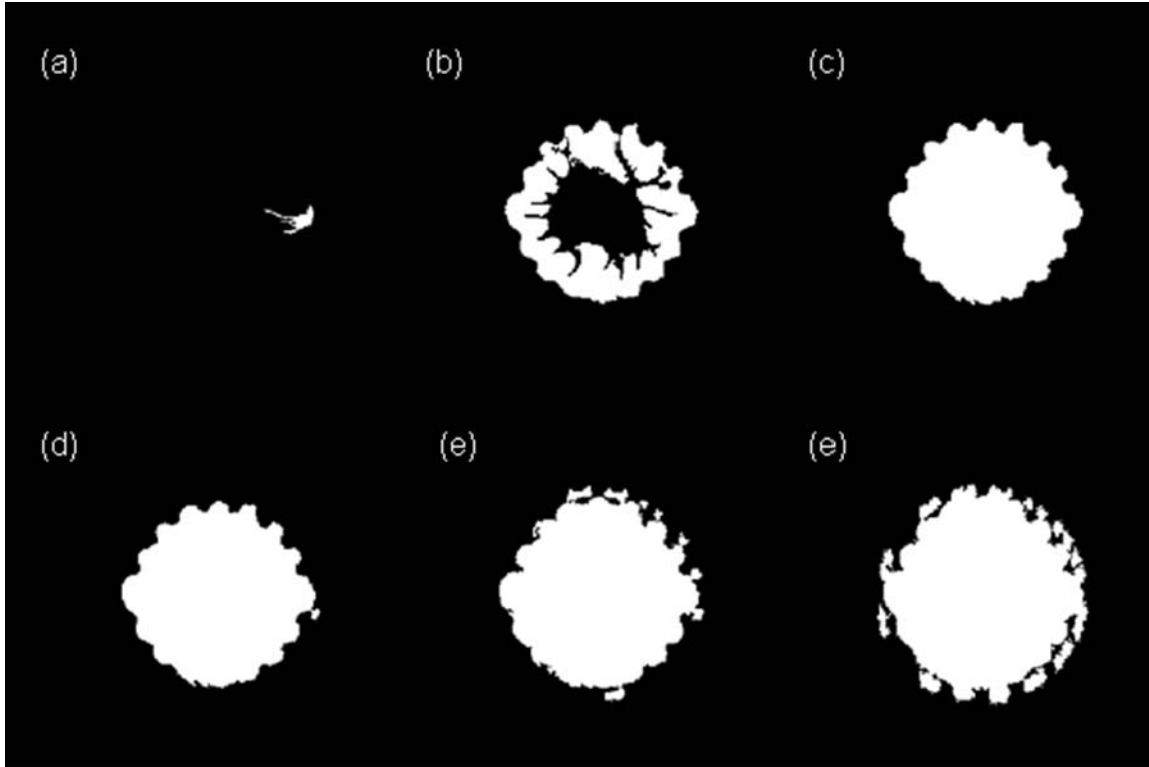


**Figure 4.4.** Subfigures (a) – (e) illustrate, the morphologically processed largest enclosed contiguous areas. The morphological operator serves to break small slivers that might connect transducer array artifacts to the breast tissue in a few early iterations.

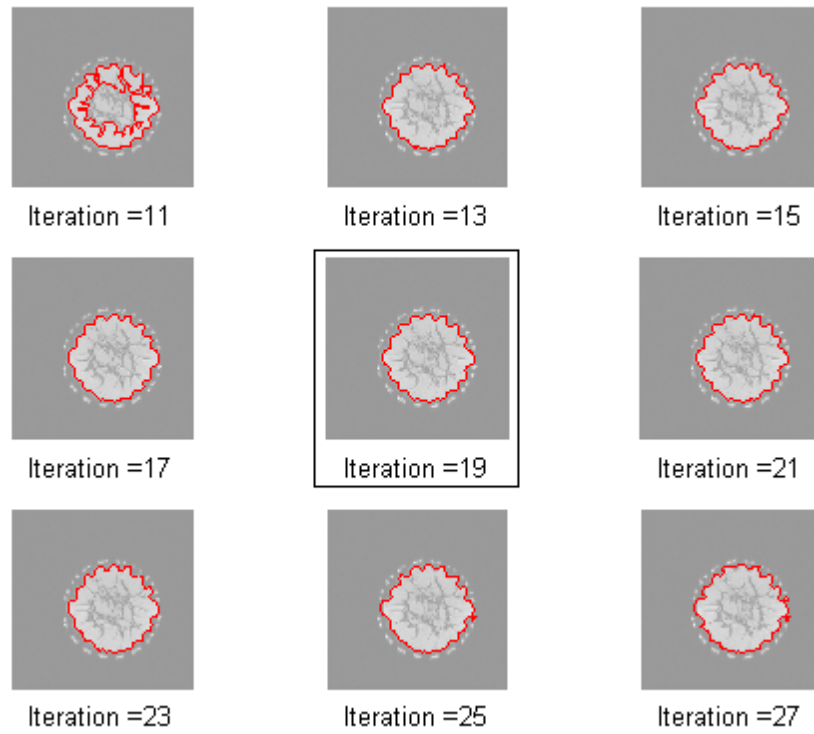


**Figure 4.5.** The ANN based prediction (highlighted) with manual override option.

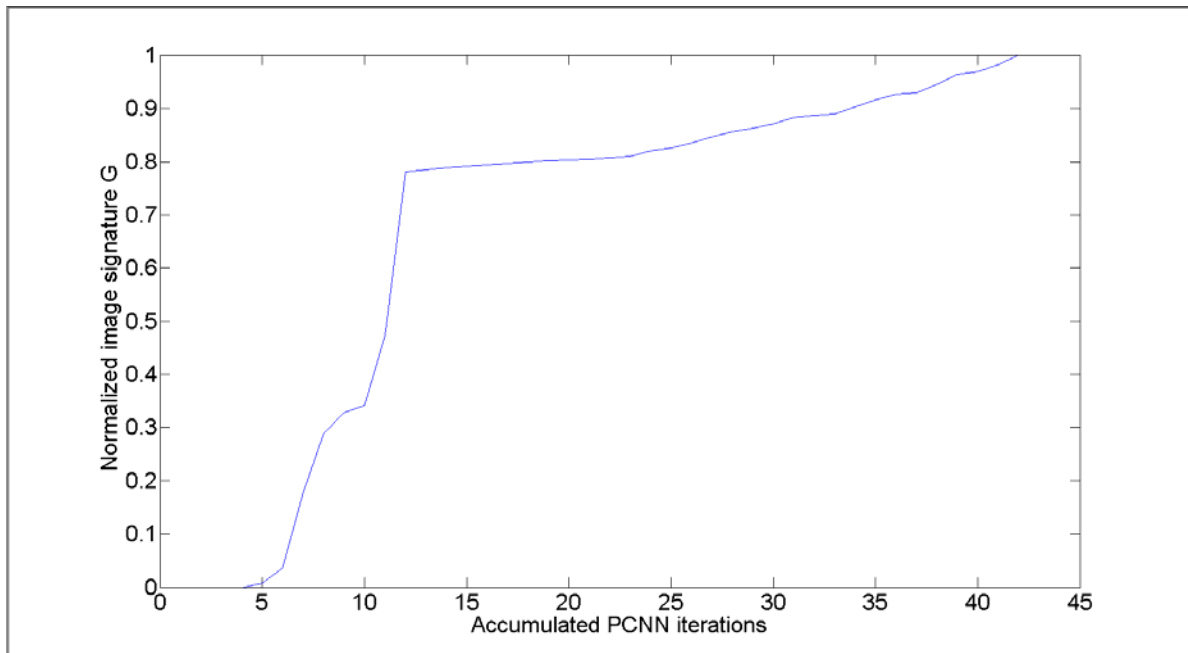


**Figure 4.6.** Illustrates the characteristic shape of the normalized image signature  $G$ . The task is to simply identify a PCNN iteration close to the beginning of the plateau region.

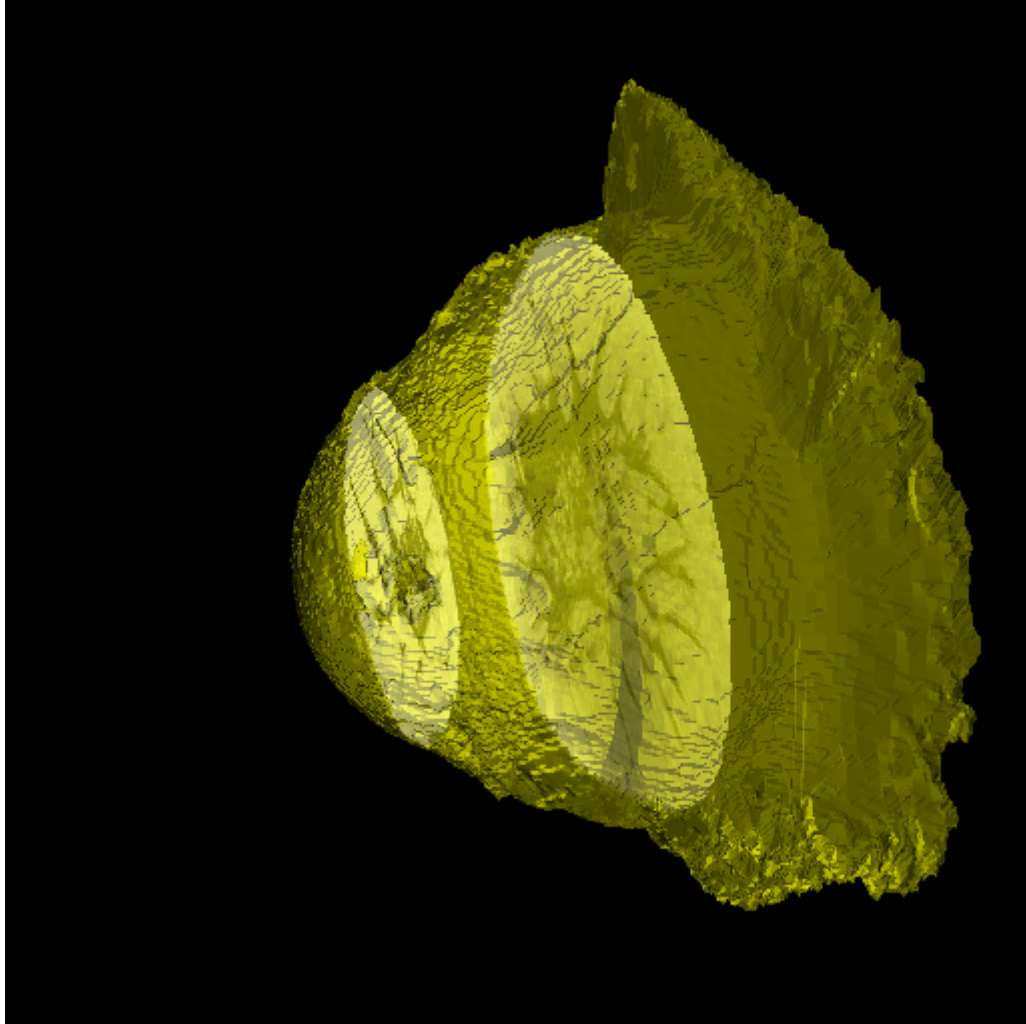


**Figure 4.7.** 3D surface mesh of the breast volume shown in Figure 4.1 with inlays of 2 sample coronal grayscale slices. The mesh was generated via the Multiple Material Marching Cubes (M3C) algorithm described by Wu and Sullivan (2003).

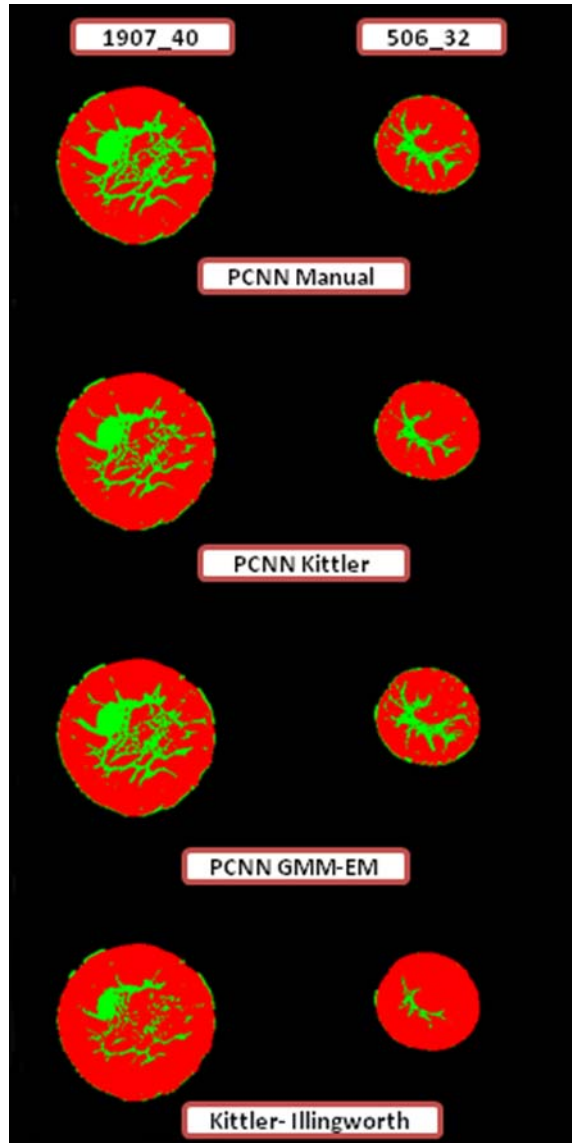


**Figure 4.8.** Qualitative results of two region segmentation algorithms on 2D slices identified by '1907\_40' and '506\_32' (Table 4.6) in columns. Figures in rows illustrate results of manual PCNN selection ('Gold' standard), PCNN-Kittler, PCNN-GMM-EM and Kittler-Illingworth thresholding algorithms. The red colored region marks adipose tissue, while the green color region encodes fibroglandular tissue.

## 4.2.2 The Eckhorn Pulse Coupled Neural Network

The PCNN operates on 2D grayscale intensity images described by variable  $S_{ij}$  with  $i, j$  describing the location of each grayscale pixel and the corresponding PCNN 'neuron'. Each PCNN neuron is directly coupled to a set of neighboring neurons encompassed by a predefined radius  $r$ , known as the 'linking field' (Waldemark, et al. 2000). The functionality is effected by means of a Feeding and Linking compartment, described by arrays  $F_{ij}$  and  $L_{ij}$ , each of dimension equaling the 2D input grayscale image, linked by two synaptic weighting matrices  $M$  and  $W$ . The synaptic weighting matrix is square with a dimension of  $(2r + 1)$  and is a normalized Gaussian about the center of the square matrix.

$$F_{ij}[n] = e^{-\alpha_F} F_{ij}[n-1] + S_{ij} + V_F (M * Y[n-1])_{ij} \quad (4.1)$$

$$L_{ij}[n] = e^{-\alpha_L} L_{ij}[n-1] + V_L (W * Y[n-1])_{ij} \quad (4.2)$$

$$U_{ij}[n] = F_{ij}[n] (1 + \beta L_{ij}[n]) \quad (4.3)$$

$$T_{ij}[n] = e^{-\alpha_T} T_{ij}[n-1] + V_T Y_{ij}[n]$$

(4.4)

$$Y_{ij}[n] = 1 \text{ if } U_{ij}[n] > T_{ij}[n] \quad (4.5)$$

$$Y_{ij}[n] = 0 \text{ if } U_{ij}[n] \leq T_{ij}[n] \quad (4.6)$$

The PCNN is implemented by iterating through equations (4.1)-( 4.6) with  $n$  as the current iteration index and ranging from 1 to  $N$  (the total number of iterations). The

matrices  $F_{ij}[0], L_{ij}[0], U_{ij}[0]$  and  $Y_{ij}[0]$  were initialized to a zero matrix, while  $T_{ij}[0]$  was initialized to a unit matrix. For each iteration, the internal activation  $U_{ij}$  is computed and compared against the threshold  $T_{ij}$ . Thus, the array  $Y_{ij}[n]$  is a binary image representing the PCNN mask at that particular iteration.

The PCNN coefficients used in this article were originally sourced from the work of Johnson and Padgett (1999) and Waldemark et al. (2000). The same constants were used for rat brain cropping (Murugavel and Sullivan Jr. 2009a).  $\alpha_F, \alpha_L, \alpha_T$  are iteration (surrogate time) constants that determine the internal state of the network effecting exponential decay and  $V_F, V_L, V_T$  are magnitude scaling terms for Feeding, Linking and Threshold components of the PCNN.  $*$  is the two dimensional convolution operator.  $\beta$  is a parameter affecting linking strength, Table 4.1.

Our implementation of the PCNN operates in the ‘accumulate’ mode: that is, each iteration sums its contributions with the previous PCNN iterations.

$$A_{ij}[n] = \sum_{k=1}^n Y_{ij}[k] \quad (4.7)$$

The process described by equation (7) can result in a non binary image  $A_{ij}$ . However, for our work the accumulated iteration  $A_{ij}[n]$  is converted into a binary image by means of a thresholding operation at unity, Figure 4.2.

Constant	PCNN coefficient	Context
$\beta$	0.2	Linking strength
$\tau_F$	0.3	Feeding decay
$\tau_L$	1	Linking decay
$\tau_T$	10	Threshold decay
$V_F$	0.01	Feeding coupling
$V_L$	0.2	Linking coupling
$V_T$	20	Magnitude scaling term for threshold
$r$	3	Radius of linking field

**Table 4.1.** The values of the PCNN coefficients used in this algorithm were derived from Johnson and Padgett (1999) and Waldemark, et al. (2000). Further coefficients  $\alpha_{F,L,T} = \ln 2 / \tau_{F,L,T}$  as described by Waldemark, et al. (2000).

#### 4.2.3 Morphological, contour operations on accumulated PCNN iterations

A binary morphological operation breaks 'narrow bridges' or clusters of pixels with a radius less than  $p$  pixels. Each pixel  $i, j$  value (0 or 1) within a PCNN iteration must be continuous in at least two orthogonal directions. That is IF  $(i \pm p, \dots, i \pm 1, i)$  is 1 AND  $(j \pm p, \dots, j \pm 1, j)$  is 1, THEN pixel  $i, j = 1$ .

Perimeters or contours of isolated islands are created. The largest area within each PCNN iteration is selected. All pixels within the selected perimeter are filled with 'ones'. This process results in only one contiguous segment for each PCNN iteration. We denote each PCNN iteration at this stage by  $C_{ij}[n]$  with iteration  $n$  ranging from  $[1, N]$ . Figure 4.4 is used to illustrate the outcome of the described morphological and contour operations on the same coronal section shown in Figure 4.1(a).

A successful breast cropping results when an appropriate PCNN iteration  $n$  is selected. A 1D time signature is constructed for the PCNN iterations similar to that of Muresan (2003). The abscissa or timeline is the iteration count. The ordinate is the total number of pixels within the largest contoured area for each PCNN iteration.

$$G[n] = \sum_{ij} C_{ij}[n]$$

Where  $n$  ranges from  $[1, N]$ . This image signature has a characteristic shape for similar images with similar regions of interest. This information is used as a surrogate time series in a traditional ANN training sequence to automatically extract the breast tissue. The maximum number of iterations ( $N$ ) of the PCNN is set to a suitable large number which allows for capturing the entire region of interest in each

slice and subject.

#### 4.2.4 Traditional ANN based selection of breast mask

A previously trained ANN receives the accumulated response as a function of iteration and outputs an iteration number,  $n$ . Multi Layer Perceptron (MLP) is a widely used (Haykin 1998) supervised, feedforward ANN model which can be trained to map a set of input data to a desired output using standard backpropagation algorithms. Since each grayscale breast coronal section  $S_{ij}$  is now represented by the PCNN iterations  $C_{ij}[n]$  with  $n$  ranging from  $[1, N]$  and an image signature  $G$ , it is possible to create a training set for the MLP.

Figure 4.6 shows the characteristic shape of the image signature for the sample mid section coronal breast slice. In the illustrated example, iteration numbers corresponding to 14 to 20 will produce very similar breast masks. This characteristic step response behavior can be fitted easily. It requires few training volumes to create a reliable trained ANN. For the work presented herein, a single breast volume with 83 individual 2D slices was sufficient to train the network. The neural architecture of the MLP used in this article consists of one input layer, one hidden layer and a single output neuron. The input layer neurons simply map to the image signature which is a vector of dimension  $N$ . The vector is normalized for the purposes of efficient supervised training using the back propagation algorithm. The hidden layer consisted of about half the number of neurons in the input layer and the

single output neuron mapped the desired PCNN iteration corresponding to the breast mask.

#### 4.2.5 Minimum Error Thresholding

This section is adapted from the multiple material segmentation work described by Murugavel and Sullivan (2009b). In this section we describe the multiple threshold clustering method proposed by Kittler and Illingworth (1986) as a possible fibroglandular – adipose tissue segmentation method. Our choice of this method is based on the quantitative results reported in the recent review paper by Sezgin and Sankur (2004), where they compared the performance of 40 different thresholding methods and ranked the method of Kittler and Illingworth (1986) as the best performer among the 40 different methods surveyed. While their tests did not involve MR images, the minimum error thresholding method has found application in initializing the FCM (Fuzzy C Means) clustering component of the unsupervised T1 weighted MRI brain segmentation algorithm proposed by Xue et al. (2003).

Consider a grayscale image  $s$ , with gray levels  $g$ , whose histogram  $h(g)$  has  $m$  modes representing a mixture of  $m$  normal densities. Kittler and Illingworth (1986) had shown the optimal separation thresholds  $X_i$  can be obtained at the minimum of the criterion,  $J$ , described by equation 4.8.

$$J(X_1, \dots, X_{m-1}) = 1 + 2 \times \sum_{i=1}^m \{P_i(X_i) [\log \sigma_i(X_i) - \log P_i(X_i)]\}, \quad (4.8)$$

where *a priori* probability  $P_i(X_i)$ , modal mean  $\mu_i(X_i)$ , and standard deviation  $\sigma_i(X_i)$  are described by equations (4.9) – (4.12).

$$P_i(X_i) = \sum_{g=X_{i-1}+1}^{X_i} h(g), \quad (4.9)$$

$$\mu_i(X_i) = \frac{1}{P_i(X_i)} \sum_{g=X_{i-1}+1}^{X_i} gh(g), \quad (4.10)$$

$$\sigma_i^2(X_i) = \frac{1}{P_i(X_i)} \sum_{g=X_{i-1}+1}^{X_i} [g - \mu_i(X_i)]^2 h(g) \quad (4.11)$$

and

$$\begin{aligned} X_m &= \text{totalNumberOfGreyLevels}, \\ X_0 &= -1. \end{aligned} \quad (4.12)$$

Murugavel and Sullivan (2009b) have extended this idea to generate a stopping criterion for the accumulated PCNN iterations. If apriori information on the number of regions,  $nRegions$ , were available, it is possible to compute the corresponding segment proportion ( $\gamma_{S_{n_i}}$ , with  $\sum_{i=1}^{nRegions} \gamma_{S_{n_i}} = 1$  and  $\gamma_{S_{n_i}} \geq 1$ ), mean ( $\mu_{S_{n_i}}$ ) and standard deviation ( $\sigma_{S_{n_i}}$ ). Since the minimum error criterion (see equation (4.8)) is based on the minimization of the Kullback Information distance (Demirkaya, et al. 2009; Haralick and Shapiro 1992), we can construct a time series representation of the multiple region segmentation as shown in equation (4.8).

$$Js(n) = 1 + 2 \times \sum_{i=1}^{nRegions} \{ \gamma_{S_{n_i}} [\log \sigma_{S_{n_i}} - \log \gamma_{S_{n_i}}] \} \quad (4.13)$$

The minimum of this function was found (Murugavel and Sullivan Jr. 2009b) to yield

the optimal segmentation among the various PCNN iterations with  $nRegions$ .

#### 4.2.6 Gaussian Mixture Model (GMM) based selection

This section is adapted from the multiple material segmentation work described by Murugavel and Sullivan (2009b). We reported highly successful segmentations of Grey Matter (GM) – White Matter (WM) and Cerebro Spinal Fluid (CSF) regions on 20 publicly (IBSR) available T1 weighted MR brain volumes. In this section, we attempt breast tissue segmentation using the same technique. A distribution describing a grayscale image  $s$ , consisting of only those pixels within the cropped breast can be modeled by a mixture of  $k$  Gaussians. This univariate mixture with pixel intensities  $x$ , can be represented as the following weighted summation of  $k$  class conditional probability distribution functions (Demirkaya, et al. 2009);

$$f(x) = \sum_{i=1}^k \gamma_i N(x | \mu_i, \sigma_i^2) \quad (4.14)$$

$$N(x | \mu_i, \sigma_i^2) = \frac{1}{(2\pi\sigma_i^2)^{\frac{1}{2}}} \exp\left(-\frac{(x - \mu_i)^2}{2\sigma_i^2}\right) \quad (4.15)$$

where  $\mu_i$ ,  $\sigma_i$ ,  $\gamma_i$  represent the mean, standard deviation and mixing proportion of

class  $i$ . with  $\sum_{i=1}^k \gamma_i = 1$  and  $\gamma_i \geq 1$ .

The standard Expectation Maximization (EM) (Dempster, et al. 1977; Bishop 1995) algorithm can be used as an estimator to generate a feature vector consisting of means, standard deviations and mixing proportions of the  $k$  Gaussians of each

grayscale image,  $\hat{e} = [\mu_1 \dots \mu_k \ \sigma_1 \dots \sigma_k \ \gamma_1 \dots \gamma_k]$ . As described in Section 4.2.5, accumulated PCNN iterations  $A[n]$  may be computed for each grayscale image  $S$ . With access to *a priori* information on the number of regions (equal to  $k$ ), we can generate a feature vector for each PCNN iteration,  $e_n = [\mu_{S_{n1}} \dots \mu_{S_{nk}} \ \sigma_{S_{n1}} \dots \sigma_{S_{nk}} \ \gamma_{S_{n1}} \dots \gamma_{S_{nk}}]$ , similar to the estimate  $\hat{e}$  from the GMM-EM formulation described in this section. In this implementation, the subscript  $n$  represents only those accumulated PCNN iterations with a total of  $k$  regions. The appropriate choice of the PCNN segmentation is simply that iteration  $n$ , which minimized the Euclidean norm  $\|\hat{e} - e_n\|$ . This strategy is unsupervised and requires no prior classifier training.

### 4.3 Experiment details

#### 4.3.1 Data

The test data consisted of 6 breast MR volumes comprising a total of 331 (256 x 256) slices obtained from Dartmouth College, NH. One of the volumes consisting of 83 slices was used to train the ANN for automatic cropping of the breast. The other 5 volumes served as test data and were manually cropped using the PCNN formulation to create the ‘Gold’ standard. Two slices from each of these volumes were selected for testing the fibroglandular – adipose segmentation algorithms described in Section 4.2.

### 4.3.2 Software specifications

All described algorithms were implemented in Matlab 2008a (Mathworks, MA, U.S.A).

### 4.3.3 Parameters employed in the ANN based cropping scheme

The algorithm employing the methods described in Section 4.2.4 is presented as a pseudo code in Table 4.2. The input grayscale breast volumes were treated as the subject data and individually referred to as 'grayscaleAnatomy' variable in Table 4.2. The PCNN algorithm was implemented and the 'PCNNInputParametersVector' of Table 4.2 contained numerical values of the various PCNN parameters,  $\alpha_F, \alpha_L, \alpha_T, \beta, V_F, V_L, V_T$ , and  $r$  described in Table 4.1. This length  $N$  of each PCNN image signature vector was set to 42. This setting ensured that the entire image space was filled by the accumulated PCNN iterations. The grayscale anatomy file was passed to the PCNN algorithm and the  $N$  binary output pulses for each slice computed, which corresponds to  $A$  of equation (4.7) and held in variable 'binaryPCNNIterations'. This data was further processed by means of a binary morphological operation to break 'bridges', as described in section 4.2.3. The value of the 'bridge' radius  $p$  was set to 2 for this study.

The neural network classifier in direct relation to the choice of the number of pulses had  $N$  input neurons, one hidden layer of 20 neurons (approximately  $0.5N$ ) and one output. For purposes of training, a single breast volume consisting of 83 slices was used. The activation function of the hidden layer was chosen to be a nonlinear hyperbolic tangent function while that of the output layer was linear. The '*newff*' and '*train*' functions available in Matlab 2008a's Neural Network toolbox V6.0 were used to train the classifier using the gradient descent with momentum backpropagation algorithm.

```

function [autoCroppedBreastVolume(nrow,ncol,nslice)] =

    autoCrop[grayscaleAnatomy(nrow,ncol,nslice), PCNNInputParametersVector, N]

for i = 1 : nslice

    for j = 1 : N

        // PCNN returns binary array A on input of S (see equations (4.1) - (4.7))

        binaryPCNNIterations(:, :, i, j) = PCNN(grayscaleAnatomy(:, :, i), PCNNInputParametersVector, j)

        // binary morphological operator to break 'narrow bridges' with a radius less than p pixels.

        binaryPCNNIterations(:, :, i, j) = breakBridges(binaryPCNNIterations(:, :, i, j), p)

        // assuming largest area of corresponding iteration contain the desired breast mask

        binaryPCNNIterations(:, :, i, j) = largestArea(binaryPCNNIterations(:, :, i, j))

        // stores image signature in vector form

        PCNNImageSignature(i, j) = area(binaryPCNNIterations(:, :, i, j))

    end

end

// determines iteration

choiceOfIteration = preTrainedNeuralNetworkClassifier(PCNNImageSignature(i, :))

autoCroppedBreastVolume(:, :, i) = binaryPCNNIterations(:, :, i, choiceOfIteration)

end

```

**Table 4.2.** Pseudo code of the automatic breast cropping algorithm

#### 4.3.4 Parameters employed in the PCNN minimum error thresholding method

The algorithm described in the PCNN based minimum error thresholding formulation described in Section 4.2.5 is presented as pseudo code in Table 4.3. The 10 cropped grayscale breast slices described in Section 4.3.1 were treated as subject data and individually addressed by the ‘croppedGrayscaleAnatomy’ variable in Table 4.3. The PCNN algorithm was implemented and the ‘PCNNInputParametersVector’ of Table 4.2 contained numerical values of the various PCNN parameters,  $\alpha_F, \alpha_L, \alpha_T, \beta, V_F, V_L, V_T$ , and  $r$  described in Table 4.1. In this implementation, the number of regions, ‘nRegions’, was set to two (adipose and fibroglandular). The PCNN time series representation, ‘kittlerIllingworthPCNNTimeSeries’ was determined for each slice based on equation (4.13). The minimum of this time series yielded the optimal segmentation among the various PCNN iterations with 2 regions.

```

function [segmentedBreastVolume(nrow,ncol,nslice)] =
autoSegPCNNTIMEseries[croppedGrayscaleAnatomy(nrow,ncol,nslice), PCNNInputParametersVector, nRegions]

for i = 1 : nslice

    // PCNN returns accumulated array A on input of S (see equations (4.1) - (4.7)). Cropped breast mask applied on each
    // iteration. Function returns only accumulated PCNN iterations with nRegions.

    accumulatedPCNNIterations =

        pcnnAccumulateMode(croppedGrayscaleAnatomy(:, :, i), PCNNInputParametersVector, nRegions)

    // Determine number of PCNN pulses in the accumulatedPCNNIterations volume

    [nrow, ncol, noPulses] = size(accumulatedPCNNIterations)

    // Initialize Kittler-Illingworth based time series vector

    kittlerIllingworthPCNNTIMEseries(1 : noPulses) = 0

    // Begin loop to compute the time series vector

    for j = 1 : noPulses

        if noRegions(accumulatedPCNNIterations(:, :, i)) == nRegions

            kittlerIllingworthPCNNTIMEseries(j) =

                computeKittlerIllingworthMeasure(accumulatedPCNNIterations(:, :, i))

        end

    end

    // Determine iteration. Select PCNN iteration corresponding to minimum of the PCNN Kittler Illingworth time series

    segmentedBreast(nrow, ncol, i) = minSelect(kittlerIllingworthPCNNTIMEseries, accumulatedPCNNIterations)

end

```

**Table 4.3.** Pseudo code of PCNN - Minimum Error Thresholding based selection method

### 4.3.5 Parameters employed in the GMM – EM based selection method

The algorithm for the GMM – EM based selection method is presented as pseudo code in Table 4.4. The 10 cropped grayscale breast slices described in Section 4.3.1 were treated as subject data and individually addressed by the ‘croppedGrayscaleAnatomy’ variable in Table 4.4. The PCNN algorithm was implemented and the ‘PCNNInputParametersVector’ of Table 4.2 contained numerical values of the various PCNN parameters,  $\alpha_F, \alpha_L, \alpha_T, \beta, V_F, V_L, V_T$ , and  $r$  described in Table 4.1. In this implementation, the number of regions, ‘nRegions’, was set to two (adipose and fibroglandular). The grayscale intensities of each individual 2D slice  $S$  were modeled as a mixture of two Gaussians and the basic EM algorithm described by the function ‘*gmm\_b\_em*’ operating with default parameters, available as part of the GMMBayes Toolbox Version 1.0 (open source GNU license, <http://www.it.lut.fi/project/gmmbayes>) was used to generate the estimated feature vector  $\hat{e} = [\mu_1 \dots \mu_k \ \sigma_1 \dots \sigma_k \ \gamma_1 \dots \gamma_k]$ . The Euclidean distance between the estimated feature vector described by the variable ‘*estimatedFeatureVector*’ and each of the individual feature vectors, described by variable ‘*featureVec*’ was computed, ‘*euclideanDistance*’. The two region segmentation for each grayscale slice  $S$  is the accumulated PCNN iteration that corresponds to the minimum of the vector, ‘*euclideanDistance*’.

```

function[segmentedBreastVolume(nrow,ncol,nslice)]

=autoSegPCNNGaussian[croppedGrayscaleAnatomy(nrow,ncol,nslice),PCNNInputParametersVector,nRegions]

for i = 1 : nslice

    // PCNN returns accumulated array A on input of S(see equations (4.1) - (4.7)). Cropped breast mask applied on each
    // iteration. Function returns only accumulated PCNN iterations with nRegions.

    S = croppedGrayscaleAnatomy(: , : , i)

    accumulatedPCNNIterations = pcnnAccumulateMode(S, PCNNInputParametersVector, nRegions)

    // Determine number of PCNN pulses in the accumulatedPCNNIterations volume

    [nrow, ncol, noPulses] = size(accumulatedPCNNIterations)

    // Estimate the means, standard deviations and mixing proportion of the nRegions (GM, WM and CSF) in S
    // [eMu1 .. eMunRegions eSD1 .. eSDnRegions eMp1 .. eMpnRegions] (see section 4.2.5)

    estimatedFeatureVector = gmmEM(S, nRegions)

    // Begin loop to compute feature vector (identical to the estimate ) for individual PCNN iterations, distance measure

    for j = 1 : noPulses

        if noRegions(accumulatedPCNNIterations(: , : , i) ) == nRegions

            // compute feature vector [Muj,1 .. Muj,nRegions SDj,1 .. SDj,nRegions Mpj,1 .. Mpj,nRegions]

            featureVec(j) = computeMeansStdDevProportions(accumulatedPCNNIterations, S)

            // Euclidean distance between estimate and computed feature vector of each iteration

            euclideanDistance(j) = euclideanNorm(estimatedFeatureVec – featureVec(j))

        end

    end

    // Begin GMM – EM based selection. Select PCNN iteration corresponding to min of euclidean distance

    segmentedBreast(nrow, ncol, i) = minSelect(euclideanDistance, accumulatedPCNNIterations)

end

```

**Table 4.4.** Pseudo code of PCNN – GMM EM based selection method

## 4.4 Results and Discussion

### 4.4.1 Breast cropping results

The PCNN based automated breast cropping algorithm was tested on 5 volumes described in Section 4.3.1. An average breast cropping including original volume input to cropped and mask outputs was completed in under 10 minutes on a Pentium 4 class machine with 4 GB RAM. Figure 7 provides a sample result from the described breast cropping algorithm.

For purposes of numerical validation, we created masks for each of the volumes by manually selecting an appropriate PCNN iteration. The manually created masks served as the ‘gold’ standard. For a quantitative metric, we employed the Jaccard’s index (Jaccard 1912). This index is a similarity measure in the range  $[0, 1]$ , where 1 describes an ideal match between the subject mask  $A_{Sub}$  generated by the proposed algorithm and the ground truth represented by the manually created mask  $M_G$  for that subject. The Jaccard similarity index is defined by:

$$Jaccard = \frac{|A_{Sub} \cap M_G|}{|A_{Sub} \cup M_G|}$$

We computed these indices using our automated PCNN algorithm for all volumes and summarized the results in Table 4.5.

#### 4.4.2 Adipose and Fibroglandular tissue segmentation results

The PCNN minimum error thresholding and PCNN – GMM – EM algorithms were tested on the 10 individual, cropped breast slices described in Section 4.3.1. Qualitative results are illustrated in Figure 4.8. The compute time for each slice is about 5 seconds on a Pentium 4 PC with 4 GB RAM. For quantitative evaluation, we manually selected masks using the PCNN algorithm, which served as the ‘Gold’ standard. For a quantitative metric we employed the Jaccard similarity index for each region. The results obtained are presented in Table 4.6. For comparison, the popular Kittler Illingworth thresholding method (see Equation 4.8) was applied on the 10 test slices and the results included in Table 4.6. A paired Student’s t-test was conducted to test the null hypothesis that difference of means between the PCNN-GMM-EM selection strategy and the control Kittler Illingworth thresholding are a random sample from a normal distribution with mean 0 and unknown variance. For Fibroglandular tissue segmentation, the one tailed test on 10 grayscale slices yielded a P value = 0.0023, rejecting the null hypothesis at a 99.5 % confidence level in support of the alternate hypothesis that the mean Jaccard index of the PCNN - GMM-EM method is higher than that of the Kittler Illingworth thresholding operation. The corresponding t value equaled -3.75. Similar tests on Adipose tissue segmentation effectively rejected the null hypothesis at a reduced 98 % confidence level, with p values equaling 0.0106 (t value = -2.78). The degrees of freedom was 9. These results showcase the PCNN as a viable cropping and two region segmentation algorithm for breast MRI. It is evident a single threshold method such

as the Kittler Illingworth method (Kittler and Illingworth 1986) is not as effective for breast MR, as fibroglandular tissue has intensity variations that would cause it to be incorrectly labeled if spatial proximity is not considered. One of the advantages of the PCNN based breast cropping method is the ability to handle 2D slices where the fibroglandular tissue is located close to the breast-air interface.

<b>Breast volume</b>	<b>PCNN cropping</b>	<b>Number of slices</b>
504	0.988	42
505	0.993	39
501c	0.996	53
1907	0.985	77
506	0.999	37

**Table 4.5.** Jaccard indices obtained on five breast volumes employing the PCNN based cropping method.

Breast slice ID	PCNN Kittler minimization		PCNN GMM EM		Kittler Thresholding	
	Fibroglandular	Adipose	Fibroglandular	Adipose	Fibroglandular	Adipose
1907_23	1.00	1.00	0.81	0.89	0.55	0.83
1907_40	0.80	0.94	0.95	0.99	0.51	0.87
501c_20	0.92	0.96	0.89	0.95	0.76	0.91
501c_50	0.90	0.95	0.91	0.96	0.76	0.90
504_13	0.87	0.96	0.80	0.92	0.40	0.84
504_34	0.45	0.89	0.58	0.83	0.43	0.88
505_11	0.82	0.94	0.78	0.91	0.30	0.81
505_24	0.35	0.78	0.75	0.86	0.27	0.76
506_13	1.00	1.00	0.48	0.92	0.70	0.98
506_32	0.66	0.93	0.86	0.96	0.26	0.85
<b>Average</b>	0.78	0.94	0.78	0.92	0.49	0.86

**Table 4.6.** Jaccard indices obtained on the 10 breast slices employed in evaluation of the PCNN minimum error thresholding, PCNN GMM – EM based formulation and the standard Kittler Illingworth (single threshold) method.

#### 4.5 Conclusion

Two PCNN based automatic cropping and adipose – fibroglandular tissue segmentation methods (PCNN – Kittler Illingworth formulation and PCNN – GMM) were described and tested on 5 MR volumes (total of 248 slices) and 10 individual cropped 2D slices. Our numerical comparison metric indicates that the PCNN, on account of its inherent intensity delineation and spatial linking characteristics, is an effective tool for handling MR breast volume segmentation tasks.

## Chapter 5

### Conclusions and Future Work

The main contribution of this dissertation is the demonstration and quantitative evaluation of the PCNN as a viable, multiple material segmentation strategy in automatically segmenting MRI volumes. This dissertation was not intended to focus on PCNN model development, but rather the design of systems that helped select a suitable PCNN iteration. To this end, the dissertation focused on MR images of the rat brain, human brain and the human breast.

A NeuroImage reviewer summarized "To date, approaches to brain extraction from rat MRI data have often involved the application of algorithms developed for Human images (with mixed results, for example, working well over only a certain rostrocaudal range of brain coverage), hand delineation (tedious, and likely operator-dependent, heuristic approaches such as intensity thresholding (non-standard and not of general applicability) or the application of a standard brain mask after co-registration (requires spatial normalization prior to masking and does not readily allow differences in brain morphology to be obtained). There has been a general lack of brain extraction algorithms designed and optimized for rat brain MRI data".

To address this niche, a novel, brain extraction algorithm was developed and tested for automatic cropping of rat brain volumes. These image masks were mapped onto a timeline curve rendering the task into an appropriate iteration selection problem. The surrogate 'time' signature was passed to a previously trained ANN for final

iteration selection. The algorithm was tested on rat brain volumes from 3 different acquisition configurations and quantitatively compared against corresponding manually created masks which served as the reference. A paired Student's t-test on results from BET V2.1 and the PCNN cropping tool supported the alternate hypothesis that the mean Jaccard index of the PCNN method is higher than that of BET V2.1 for the 4.7 T anatomy (256x256) dataset at a 99.999% confidence level. Our results conclusively demonstrate that PCNN based brain extraction represents a unique, viable fork in the lineage of the various brain extraction strategies.

The PCNN code and data (4.7T 256×256×12 anatomy volumes, 'Gold' standard masks) described in the dissertation was made available as a supplementary download (NeuroImage/Elsevier web products server) on a 'Non profit, academic/research use only' type of license.

In chapter three we addressed the problem of segmenting human brains. Two novel PCNN based algorithms (PCNN – ANN, PCNN – GMM EM) were developed and tested for automatic segmentation of human T1 weighted MRI brain volumes. These were bench marked against data publically available at Harvard's Internet Brain Segmentation Repository. The PCNN – ANN based selection method introduced the concept of a 1D time series representation of a 2D multiple material segmentation task. A paired Student's t-test was conducted to test the null hypothesis that difference of means between the PCNN-GMM-EM selection strategy and previously proposed methods (Maximum Likelihood, tree-structure k-means) are

a random sample from a normal distribution with mean 0 and unknown variance. For GM, the one tailed test on 20 volumes yielded a P value  $< 0.0001$  for both methods (Maximum Likelihood, tree-structure k-means), effectively rejecting the null hypothesis at a 99.999 % confidence level in support of the alternate hypothesis that the mean Jaccard index of the PCNN- GMM-EM method is higher than that of Maximum Likelihood and tree structure k-means. Similar tests on WM segmentation effectively rejected the null hypothesis at a reduced 95 % confidence level, with p values equaling 0.0101 and 0.0244 respectively for the Maximum Likelihood and tree structure k-means methods.

Our quantitative results on human brain volumes demonstrated that PCNN based multiple material segmentation strategies can approach a human eye's intensity delineation capability in grayscale image segmentation tasks.

Our survey of literature revealed that there are no specific tools designed for automatic breast cropping and segmentation. This dissertation has generated specific tools and datasets to address this issue. The PCNN –ANN method, PCNN – Kittler Illingworth formulation and the PCNN – GMM method were adapted for cropping and segmenting human breast volumes. A paired Student's t-test was conducted to test the null hypothesis that difference of means between the PCNN- GMM-EM selection strategy and the control Kittler Illingworth thresholding are a random sample from a normal distribution with mean 0 and unknown variance. For Fibroglandular tissue segmentation, the one tailed test on 10 grayscale slices

yielded a P value of 0.0023, rejecting the null hypothesis at a 99.5 % confidence level in support of the alternate hypothesis that the mean Jaccard index of the PCNN-GMM-EM method is higher than that of the Kittler Illingworth thresholding operation. Similar tests on Adipose tissue segmentation effectively rejected the null hypothesis at a reduced 98 % confidence level, with p values equaling 0.0106. The degrees of freedom were 9.

These results showcase the PCNN as a viable cropping and two region segmentation algorithm for breast MRI.

### **Future Work**

Rat brain cropping: A centroid based selection strategy for cropping rat brain volumes needs to be incorporated for regions beyond the +6 mm to -11 mm AP (with reference to the Paxinos Atlas) region. To improve the cropping results, the PCNN algorithm could be employed in a hybrid configuration to initiate a model based cropping algorithm, such as an active contours formulation. Information from neighboring slices could be used to improve the cropping by computing the Jaccard index between consecutive cropped slices. It is evident that the difference in the Jaccard indices between consecutive slices should be within a small threshold. Any local sequence of slices that violates this threshold setting could be subjected to a more aggressive bridge breaking operator, before re-computing the 'time signature' and updating the prediction.

Human brain segmentation: Prior information from tissue probability maps can be used to train two different classifiers (GM-WM, 'GM-WM' and CSF) depending on the *a priori* prediction of the number of classes in a particular 2D grayscale slice. Currently the PCNN constants have been sourced from Johnson and Padgett (1999) and Waldemark et al. (2000). The performance of the PCNN algorithm could perhaps be improved by optimizing PCNN parameters for specific tasks. A closed loop formulation that tracks a predefined 'time signature', while updating PCNN parameter gains would be a significant update to the proposed segmentation method.

A breast segmentation repository similar to that of IBSR is currently lacking. We hope to address this via our collaborators at Dartmouth College, NH. Objective evaluation of multiple segmentation algorithms on breast data similar to the Sezgin and Sankur (2004) paper will follow. The PCNN needs to be evaluated as a tumor segmentation strategy.

## References

- Aboutanos, G.B., Nikanne, J., Watkins, N., Dawant, B.M., 1999. Model creation and deformation for the automatic segmentation of the brain in MR images. *IEEE Transactions on Bio-Medical Engineering* 46(11):1346-1356.
- Ashburner J. and Friston K. J. 2005. Unified segmentation. *NeuroImage* 26(3):839-851.
- Battaglini, M., Smith S.M., Brogi, S., De Stefano, N., 2008. Enhanced brain extraction improves the accuracy of brain atrophy estimation. *NeuroImage* 40, 583-589.
- Beckmann, C.F., Jenkinson, M., Woolrich, M.W., Behrens, T.E. J., Flitney, D.E., Devlin, J.T., Smith, S.M., 2006. Applying FSL to the FIAC data: Model-based and model-free analysis of voice and sentence repetition priming. *Human Brain Mapping* 27, 380-391.
- Belardinelli, P., Mastacchi, A., Pizzella, V., Romani, G.L., 2003. Applying a visual segmentation algorithm to brain structures MR images. *Conference proceedings of the First International IEEE EMBS Conference on Neural Engineering*, 507-510.
- Behrens S., Laue H., Althaus M., Boehler T., Kuemmerlen B., Hahn H. K., Peitgen H. 2007. Computer assistance for MR based diagnosis of breast cancer: Present and future challenges. *Computerized Medical Imaging and Graphics* 31(4-5):236-247.
- Bishop, C. M., 1995. *Neural networks for pattern recognition*. Clarendon Press, Oxford.
- Brooksby B., Pogue B. W., Jiang S., Dehghani H., Srinivasan S., Kogel C., Tosteson T. D., Weaver J., Poplack S. P., Paulsen K. D. 2006. Imaging breast adipose and fibroglandular tissue molecular signatures by using hybrid MRI-guided near-infrared spectral tomography. *Proceedings of the National Academy of Sciences* 103(23):8828-8833.
- Canals, S., Beyerlein, M., Murayama, Y., Logothetis, N.K., 2008. Electric stimulation fMRI of the perforant pathway to the rat hippocampus. *Magnetic Resonance Imaging* 26, 978-986.
- Caulfield, H.J. and Kinser, J.M., 1999. Finding the shortest path in the shortest time using PCNN's. *IEEE Transactions on Neural Networks* 10, 604-606.
- Cocosco C. A., Zijdenbos A. P., Evans A. C. 2003. A fully automatic and robust brain MRI tissue classification method. *Medical Image Analysis* 7(4):513-527.

- Congorto, S., Penna, S.D., Erne, S.N., 1996. Tissue segmentation of MRI of the head by means of a kohonen map. Engineering in Medicine and Biology Society, 1996. Bridging Disciplines for Biomedicine. Proceedings of the 18th Annual International Conference of the IEEE 3, 1087-1088.
- Dale, A.M., Fischl, B., Sereno, M.I., 1999. Cortical surface-based analysis: I. segmentation and surface reconstruction. *NeuroImage* 9, 179-194.
- Demirkaya, O., Asyali, M. H., Sahoo, P. K., 2009. Image processing with Matlab, applications in medicine and biology, CRC Press.
- Dempster, A. P., Laird, N. M., Rubin, D. B., 1977. Maximum Likelihood from Incomplete Data via the EM Algorithm. *Journal of the Royal Statistical Society, Series B (Methodological)*, 39(1):1-38.
- Dogdas, B., Shattuck, D.W., Leahy, R.M., 2005. Segmentation of skull and scalp in 3-D human MRI using mathematical morphology. *Human Brain Mapping* 26, 273-285.
- Duda, R. and Hart, P., 1973. Pattern Classification and Scene Analysis. Wiley-Interscience.
- Dyrby, T.B., Rostrup, E., Baaré, W.F.C., van Straaten, E.C.W., Barkhof, F., Vrenken, H., Ropele, S., Schmidt, R., Erkinjuntti, T., Wahlund, L., Pantoni, L., Inzitari, D., Paulson, O.B., Hansen, L.K., Waldemar, G., 2008. Segmentation of age-related white matter changes in a clinical multi-center study. *NeuroImage* 41, 335-345.
- Eckhorn, R., Reitboeck, H.J., Arndt, M., Dicke, P., 1990. Feature linking via synchronization among distributed assemblies: Simulations of results from cat visual cortex. *Neural Computation* 2, 293-307.
- Egmont-Petersen, M., de Ridder, D., Handels, H., 2002. Image processing with neural networks—a review. *Pattern Recognition* 35, 2279-2301.
- Ertayş G., Gülçür H. Ö., Osman O., Uçan O. N., Tunacı M., Dursun M. 2008. Breast MR segmentation and lesion detection with cellular neural networks and 3D template matching. *Computers in Biology and Medicine* 38(1):116-126.
- Fennema-Notestine, C., Ozyurt, I.B., Clark, C.P., Morris, S., Bischoff-Grethe, A., Bondi, M.W., Jernigan, T.L., Fischl, B., Ségonne, F., Shattuck, D.W., Leahy, R.M., Rex, D.E., Toga A.W., Zou, K.H., Brown, G.G., 2006. Quantitative evaluation of automated skull-stripping methods applied to contemporary and legacy images: Effects of diagnosis, bias correction, and slice location. *Human Brain Mapping* 27, 99-113.
- Ferris, C.F., Kulkarni, P., Sullivan, J.M., Jr., Harder, J.A., Messenger, T.L., Febo, M., 2005. Pup suckling is more rewarding than cocaine: Evidence from functional magnetic resonance imaging and three-dimensional computational analysis. *Journal of Neuroscience* 25, 149-156.

FSL Frequently Asked Questions, [http://www.fmrib.ox.ac.uk/fslfaq/#bet\\_animal](http://www.fmrib.ox.ac.uk/fslfaq/#bet_animal)

Gong, Y. and Brady, M., 2008. Texture-based simultaneous registration and segmentation of breast DCE-MRI. *Digital Mammography* , 174-180.

Grachev, I.D., Berdichevsky, D., Rauch, S.L., Heckers, S., Kennedy, D.N., Caviness, V.S., Alpert, N.M., 1999. A method for assessing the accuracy of intersubject registration of the human brain using anatomic landmarks. *NeuroImage* 9, 250-268.

Gu, X., Yu, D., Zhang, L., 2004. Image thinning using pulse coupled neural network. *Pattern Recognition Letters* 25, 1075-1084.

Hawkins, J., Blakeslee, S., 2008. *On Intelligence*, Holtzbrinck/Henry Holt & Co.

Haralick, R. M. and Shapiro, L. G., 1992. *Computer and Robot Vision*. Addison-Wesley, Reading, MA.

Haykin, S., 1998. *Neural networks: A comprehensive foundation*, Prentice Hall PTR, Upper Saddle River, NJ.

Hill, A., Mehnert, A., Crozier, S., 2008. Edge intensity normalization as a bias field correction during balloon snake segmentation of breast MRI. *Engineering in Medicine and Biology Society*, 2008. EMBS 2008. 30th Annual International Conference of the IEEE , 3040-3043.

Ibrahim M., John N., Kabuka M., Younis A. 2006. Hidden markov models-based 3D MRI brain segmentation. *Image and Vision Computing* 24(10):1065-1079.

IBSR, <http://www.cma.mgh.harvard.edu/ibsr/>

IBSR publications, <http://www.cma.mgh.harvard.edu/ibsr/PubsUsingIBSR.html>

IBSR simulated data, <http://www.cma.mgh.harvard.edu/ibsr/sec3.sub1.html>

Jaccard, P., 1912. The distribution of the flora in the alpine zone. *New Phytologist* 11(2):37-50.

Jimenez-Alaniz J. R., Medina-Banuelos V., Yanez-Suarez O. 2006. Data-driven brain MRI segmentation supported on edge confidence and a priori tissue information. *IEEE Transactions on Medical Imaging* 25(1):74-83.

Johnson, J.L., Padgett, M.L., 1999. PCNN models and applications. *IEEE Transactions on Neural Networks* 10, 480-498.

Kelemen, A., Szekely, G., Gerig, G., 1999. Elastic model-based segmentation of 3-D neuroradiological data sets. *IEEE Transactions on Medical Imaging* 18, 828-839.

Keller, P., 1988. *Basic Principles of MR Imaging*, GE Medical Systems, Milwaukee, WI.

- Keller, P.E. and McKinnon, A.D., 1999. Segmentation of medical imagery with pulse-coupled neural networks. *Neural Networks*, 1999. IJCNN '99. International Joint Conference on 4, 2659-2663 vol.4.
- Kittler J. and Illingworth J. 1986. Minimum error thresholding. *Pattern Recognition* 19(1):41-47.
- Klifa, C., Carballido-Gamio, J., Wilmes, L., Laprie, A., Lobo, C., DeMicco, E., Watkins, M., Shepherd, J., Gibbs, J., Hylton, N., 2004. Quantification of breast tissue index from MR data using fuzzy clustering. *Engineering in Medicine and Biology Society*, 2004. IEMBS '04. 26th Annual International Conference of the IEEE 1, 1667-1670.
- Kovacevic, N., Lobaugh, N.J., Bronskill, M.J., Levine, B., Feinstein, A., Black, S.E., 2002. A robust method for extraction and automatic segmentation of brain images. *NeuroImage* 17, 1087-1100.
- Kuntimad, G., Ranganath, H.S., 1999. Perfect image segmentation using pulse coupled neural networks. *IEEE Transactions on Neural Networks* 10, 591-598.
- Lee, A., Rajagopal, V., Bier, P., Nielsen, P.M.F., Nash, M.P., 2009. Correlation of breast image alignment using biomechanical modeling. *Proceedings SPIE*, Volume 7262, 726219.
- Lee, C., Huh, S., Ketter, T.A., Unser, M., 1998. Unsupervised connectivity-based thresholding segmentation of midsagittal brain MR images. *Computers in Biology and Medicine* 28, 309-338.
- Lee, J., Yoon, U., Nam, S.H., Kim, J., Kim, I., Kim, S.I., 2003. Evaluation of automated and semi-automated skull-stripping algorithms using similarity index and segmentation error. *Computers in Biology and Medicine* 33, 495-507.
- Lemieux, L., Hagemann, G., Krakow, K., Woermann, F.G., 1999. Fast, accurate, and reproducible automatic segmentation of the brain in T1-weighted volume MRI data. *Magnetic Resonance in Medicine : Official Journal of the Society of Magnetic Resonance in Medicine / Society of Magnetic Resonance in Medicine* 42, 127-135.
- Lindblad, T., Kinser, J.M., 2005. *Image processing using pulse-coupled neural networks*. Springer-Verlag Inc., New York, NY.
- Littlewood, C.L., Cash, D., Dixon, A.L., Dix, S.L., White, C.T., O'Neill, M.J., Tricklebank, M., Williams, S.C.R., 2006. Using the BOLD MR signal to differentiate the stereoisomers of ketamine in the rat. *NeuroImage* 32, 1733-1746.
- Liu J. and Udupa J. K. 2009. Oriented active shape models. *Medical Imaging, IEEE Transactions on* 28(4):571-584.

- Lowe, A.S., Beech, J.S., Williams, S.C.R., 2007. Small animal, whole brain fMRI: Innocuous and nociceptive forepaw stimulation. *NeuroImage* 35, 719-728.
- Lu, H., Xi, Z., Gitajn, L., Rea, W., Yang, Y., Stein, E. A., 2007. Cocaine-induced brainactivation detected by dynamic manganese-enhanced magnetic resonance imaging (MEMRI). *Proceedings of the National Academy of Sciences* 104,2489-2494.
- Lu, H., Yang, S., Zuo, Y., Demny, S., Stein, E. A., Yang, Y., 2008. Real-time animal functional magnetic resonance imaging and its application to neuropharmacological studies. *Magnetic Resonance Imaging*, In Press, Corrected Proof.
- Ludwig, R., Bodgdanov, G., King, J., Allard, A., Ferris, C. F., 2004. A dual RF resonator system for high-field functional magnetic resonance imaging of small animals. *Journal of Neuroscience Methods* 132, 125-135.
- Marroquin J. L., Vemuri B. C., Botello S., Calderon E., Fernandez-Bouzas A. 2002. An accurate and efficient bayesian method for automatic segmentation of brain MRI. *IEEE Transactions on Medical Imaging* 21(8):934-945.
- Maryam Hasanzadeh S. K. 2008. Fuzzy image segmentation using membership connectedness. *EURASIP Journal on Advances in Signal Processing* .
- Mikheev, A., Nevsky, G., Govindan, S., Grossman, R., Rusinek, H., 2008. Fully automatic segmentation of the brain from T1-weighted MRI using bridge burner algorithm. *Journal of Magnetic Resonance Imaging* 27, 1235-1241.
- Muresan, R.C. 2003. Pattern recognition using pulse-coupled neural networks and discrete fourier transforms. *Neurocomputing* 51, 487-493.
- Murugavel M. and Sullivan Jr. J. M. 2009. Automatic cropping of MRI rat brain volumes using pulse coupled neural networks. *NeuroImage* 45(3):845-854.
- Murugavel M. and Sullivan Jr. J. M. 2009b. Multiple region segmentation using pulse coupled neural networks. *NeuroImage* Submitted.
- Nakamura K. and Fisher E. 2009. Segmentation of brain magnetic resonance images for measurement of gray matter atrophy in multiple sclerosis patients. *NeuroImage* 44(3):769-776.
- Nie K., Chen J., Chan S., Chau M. I., Yu H. J., Bahri S., Tseng T., Nalcioglu O., Su M. 2008. Development of a quantitative method for analysis of breast density based on three-dimensional breast MRI. *Medical Physics* 35(12):5253-5262.
- Otsu N. 1979. A threshold selection method from gray-level histograms. *IEEE Transactions on Systems, Man, and Cybernetics* 9(1):62.
- Paulsen, K. D., Meaney, P. M., Gilman, L. C., 2005. *Alternate breast imaging*, Springer, New York, NY.

- Paxinos, G., Watson, C., 1998. The rat brain in stereotaxic coordinates, 4th ed. Academic Press, San Diego.
- Pfefferbaum, A., Adalsteinsson, E., Sullivan, E.V., 2004. In vivo structural imaging of the rat brain with a 3-T clinical human scanner. *Journal of Magnetic Resonance Imaging* 20, 779-785.
- Pham, D.L., Xu, C., Prince, J.L., 2000. Current methods in medical image segmentation. *Annual Review of Biomedical Engineering* 2, 315-337.
- Plewes D. B., Bishop J., Samani A., Sciarretta J., Donald B Plewes, Jonathan Bishop, Abbas Samani and Justin Sciarretta. 2000. Visualization and quantification of breast cancer biomechanical properties with magnetic resonance elastography. *Physics in Medicine and Biology* 45(6):1591.
- Powell, S., Magnotta, V.A., Johnson, H., Jammalamadaka, V.K., Pierson, R., Andreasen, N.C., 2008. Registration and machine learning-based automated segmentation of subcortical and cerebellar brain structures. *NeuroImage* 39, 238-247.
- Rajapakse J. C. and Kruggel F. 1998. Segmentation of MR images with intensity inhomogeneities. *Image and Vision Computing* 16(3):165-180.
- Reddick, W.E., Glass, J.O., Cook, E.N., Elkin, T.D., Deaton, R.J., 1997. Automated segmentation and classification of multispectral magnetic resonance images of brain using artificial neural networks. *IEEE Transactions on Medical Imaging* 16, 911-918.
- Rehm, K., Schaper, K., Anderson, J., Woods, R., Stoltzner, S., Rottenberg, D., 2004. Putting our heads together: A consensus approach to brain/non-brain segmentation in T1-weighted MR volumes. *NeuroImage* 22, 1262-1270.
- Reichenbach, J. R., Przetak, Ch., Klinger, G., Kaiser, W. A., 1998. Differentiation and Segmentation of Breast Tissue Components in MR Images, Proceedings of the ISMRM 6<sup>th</sup> scientific meeting, Sydney.
- Reichenbach J., Przetak C., Klinger G., Kaiser W. A. 1999. Assessment of breast tissue changes on hormonal replacement therapy using MRI: A pilot study. *Journal of Computer Assisted Tomography* 23(3) 407-413.
- Rex, D.E., Shattuck, D.W., Woods, R.P., Narr, K.L., Luders, E., Rehm, K., Stolzner, S.E., Rottenberg, D.A., Toga, A.W., 2004. A meta-algorithm for brain extraction in MRI. *NeuroImage* 23, 625-637.
- Rivera M., Ocegueda O., Marroquin J. L. 2007. Entropy-controlled quadratic markov measure field models for efficient image segmentation. *IEEE Transactions on Image Processing* 16(12):3047.

- Roberts, T.J., Price, J., Williams, S.C.R., Modo, M., 2006. Preservation of striatal tissue and behavioral function after neural stem cell transplantation in a rat model of Huntington's disease. *Neuroscience* 139, 1187-1199.
- Rogers L. F. 2002. Impact factor: The numbers game. *American Journal of Roentgenology* 178(3):541-542.
- Schnack H. G., Hulshoff Pol H. E., Baaré W. F. C., Staal W. G., Viergever M. A., Kahn R. S. 2001. Automated separation of gray and white matter from MR images of the human brain. *NeuroImage* 13(1):230-237.
- Samani A., Bishop J., Yaffe M. J., Plewes D. B. 2001. Biomechanical 3-D finite element modeling of the human breast using MRI data. *IEEE Transactions on Medical Imaging* 20(4):271-279.
- Schnack H. G., Hulshoff Pol H. E., Baaré W. F. C., Staal W. G., Viergever M. A., Kahn R. S. 2001. Automated separation of gray and white matter from MR images of the human brain. *NeuroImage* 13(1):230-237.
- Schwarz, A.J., Gozzi, A., Reese, T., Bifone, A. 2007. In vivo mapping of functional connectivity in neurotransmitter systems using pharmacological MRI. *NeuroImage*, 34, 1627-1636.
- Schwarz, A.J., Danckaert, A., Reese, T., Gozzi, A., Paxinos, G., Watson, C., Merlo-Pich, E.V., Bifone, A., 2006. A stereotaxic MRI template set for the rat brain with tissue class distribution maps and co-registered anatomical atlas: Application to pharmacological MRI. *NeuroImage* 32, 538-550.
- Ségonne, F., Dale, A.M., Busa, E., Glessner, M., Salat, D., Hahn, H.K., Fischl, B., 2004. A hybrid approach to the skull stripping problem in MRI. *NeuroImage* 22, 1060-1075.
- Sezgin M. and Sankur B. 2004. Survey over image thresholding techniques and quantitative performance evaluation. *J.Electron.Imaging* 13(1):146-168.
- Shan Shen, Sandham W., Granat M., Sterr A. 2005. MRI fuzzy segmentation of brain tissue using neighborhood attraction with neural-network optimization. *IEEE Transactions on Information Technology in Biomedicine* 9(3):459-467.
- Sharief, A.A., Badea, A., Dale, A.M., Johnson, G.A., 2008. Automated segmentation of the actively stained mouse brain using multi-spectral MR microscopy. *NeuroImage* 39, 136-145.
- Shattuck, D.W., Sandor-Leahy, S.R., Schaper, K.A., Rottenberg, D.A., Leahy, R.M., 2001. Magnetic resonance image tissue classification using a partial volume model. *NeuroImage* 13, 856-876.
- Smith, S.M., 2002. Fast robust automated brain extraction. *Human Brain Mapping* 17, 143-155.

- Solomon J., Butman J. A., Sood A. 2006. Segmentation of brain tumors in 4D MR images using the hidden markov model. *Computer Methods and Programs in Biomedicine* 84(2-3):76-85.
- Spenger, C., Josephson, A., Klason, T., Hoehn, M., Schwindt, W., Ingvar, M., Olson, L., 2000. Functional MRI at 4.7 tesla of the rat brain during electric stimulation of forepaw, hindpaw, or tail in single- and multislice experiments. *Experimental Neurology* 166, 246-253.
- Swanson, L.W., 1998. *Brain maps : Structure of the rat brain : A laboratory guide with printed and electronic templates for data, models and schematics*, 2nd rev. ed. Elsevier, Amsterdam.
- Umbaugh, S. E., 2005. *Computer imaging: digital image analysis and processing*. CRC Press, Taylor & Francis Group, Boca Raton, FL.
- Twellmann T., Lichte O., Nattkemper T. W. 2005. An adaptive tissue characterization network for model-free visualization of dynamic contrast-enhanced magnetic resonance image data. *IEEE Transactions on Medical Imaging* 24(10):1256-1266.
- Wagenknecht, G., Belitz, H., Wolff, R., Castellanos, J., 2006. Segmentation of ROIs/VOIs from small animal images for functional analysis. *Nuclear Instruments and Methods in Physics Research Section A: Accelerators, Spectrometers, Detectors and Associated Equipment* 569, 481-487.
- Waldemark, K., Lindblad, T., Becanovic, V., Guillen, J.L.L., Klingner, P.L., 2000. Patterns from the sky: Satellite image analysis using pulse coupled neural networks for pre-processing, segmentation and edge detection. *Pattern Recognition Letters* 21, 227-237.
- Wei J., Chan H., Helvie M., Roubidoux M., Sahiner B., Hadjiiski L., Zhou C., Paquerault S., Chenevert T., Goodsitt M. 2004. Correlation between mammographic density and volumetric fibroglandular tissue estimated on breast MR images. *Medical Physics* 31(4):933-942.
- Wolters, C.H., Kuhn, M., Anwander, A., Reitzinger, S., 2002. A parallel algebraic multigrid solver for finite element method based source localization in the human brain. *Computing and Visualization in Science* 5, 165-177.
- Wu, Z., Sullivan, J.M., Jr., 2003. Multiple material marching cubes algorithm. *International Journal for Numerical Methods in Engineering* 58, 189-207.
- Xue J., Pizurica A., Philips W., Kerre E., Van De Walle R., Lemahieu I. 2003. An integrated method of adaptive enhancement for unsupervised segmentation of MRI brain images. *Pattern Recognition Letters* 24(15):2549-2560.
- Zhuang, A.H., Valentino, D.J., Toga, A.W., 2006. Skull-stripping magnetic resonance brain images using a model-based level set. *NeuroImage* 32, 79-92.

Zijdenbos A. P., Forghani R., Evans A. C. 2002. Automatic "pipeline" analysis of 3-D MRI data for clinical trials: Application to multiple sclerosis. IEEE Transactions on Medical Imaging 21(10):1280-1291.